The electron affinity of Po: a theoretical electron correlation study

FYP415
Bachelor Thesis

Lydia Armini
gusarmly@student.gu.se

GÖTEBORGS
UNIVERSITET

Supervisors: Jon Grumer (Theoretical Astrophysics, Uppsala University)
Dag Hanstorp (Physics, University of Gothenburg)

Physics, University of Gothenburg
Göteborg, June 25, 2023

Abstract

The electron affinity (EA) of polonium (Po) is calculated with the multi-configuration Dirac-Hartree-Fock (MCDHF) method combined with a relativistic configuration-interaction (RCI) approach. Po is of particular interest as one of the few remaining elements with no experimental value for its EA. There are also relatively few theoretical studies for Po, targeting these properties. The latest calculation using MCDHF is over 10 years old and newer coupled-cluster studies indicate that this value is underestimating the EA. Earlier this year, a proposal was made to CERN to perform measurements on the EA of Po and it is expected that these experiments will take place in the foreseeable future. Hence, it is now important to analyze the discrepancy between the theoretical results by testing new MCDHF atomic structure correlation models. This work also serves as a preparatory study for future calculations of the isotope shift (IS) of the EA of Po. The IS in turn directly relates to the nuclear structure of Po. The results from the present study are compared to the prior theoretical estimates of the EA and the difficulties with treating and balancing correlation in Po and Po^- will be discussed. The calculations performed estimates the EA to be 1.446 eV.

Contents

1. Introduction

The scientific field of negative ions, also referred to as anions, started with the discovery of the electron in the late 19^{th} century by J.J. Thomson. By measuring the deflection of cathode rays under the influence of electromagnetic fields, he concluded that atoms must contain even smaller constituents of negative charge, which we today call electrons. Soon after the discovery of the electron, Thomson was able to detect negative ions in his gas discharge tubes [1]. Since then, the model of the atom has been refined through subsequent experiments along with the development of quantum mechanics. In present day theory, the atom is described by a many-electron wave function whose square modulus represents the electron charge density. The force that binds the electrons to the system arises from the electrostatic attraction between the electrons and the protons in the nucleus. This description works well with neutral atoms and positively charged ions, but for anions, things become somewhat more complicated. Due to the nucleus being more effectively shielded by the other electrons for the negative ion, the r^{-1} asymptotic attraction as $r \to \infty$ is insufficient to bind the additional electron to nucleus. Instead, the existence of negative ions relies on a much weaker r^{-4} dipole potential [2]. This makes anions interesting from a fundamental theoretical perspective and the negative ionic charge also makes them useful in applications in different areas of physics.

Even though negative ions form fragile systems, they have proven to play a major role in many important physical processes. Multiple examples can be found in several scientific fields, such as astro- and plasma-physics. Already in 1939, it was proposed that H^- could explain the visible opacity in certain types of stars including the sun. Likewise, H^- is believed to have helped with stellar formation in the early stages of the universe with H^- being an intermediate step in the formation of hydrogen gas H_2 [3]. There are also several techniques commonly used in chemistry and physics which take advantage of the unique properties of negative ions. As an example, high energy beams of negative ions are used in accelerator mass spectrometry and is especially helpful when measuring the abundance of ^{14}C [4]. Since nitrogen does not form negative ions, this help reduce the background levels of the isotope ^{14}N. From a theoretical standpoint, the relatively weak central potential compared to the electron-electron interaction makes negative ions especially suitable systems to study electron correlation effects. Experimental results on atomic properties of negative ions can thus be used to benchmark theoretical models.

Another consequence of negative ions being weakly bound systems, is that only around 80% of all elements are able to form stable negative ions [2]. The availability and quality of the atomic structure studies for these elements varies. Polonium ($Z = 84$) is an element which is difficult to study in a normal laboratory setting since the atom is highly radioactive. Therefore, relatively few studies targeting atomic structure properties have been performed on Po. This is a part of the explanation why Po is one of the few remaining elements with no known experimental value for its electron affinity. Earlier this year, a proposal to perform new experiments with the aim to measure the EA was presented to the committee for the isotope facility ISOLDE at CERN [5]. Prior

attempts to measure the EA have been unsuccessful due to Po^- not being produced in sufficiently large quantities. The method previously used for producing radioactive negative ions is suitable for atoms with an EA above 2.6 eV and theoretical calculations made with the relativistic coupled-cluster approach [CCSD(T)] predict a value of 1.469 eV for the EA [5][6]. By using a different technique in which a beam of Po^+ is converted to Po^- through double electron capture is believed to yield a more effective production of Po^-. The EA will be determined using laser photodetachment spectroscopy and if the experiment is successful, a high precision measurement of the EA will be obtained.

As mentioned above, the most recent calculation made by Borschevsky *et al.* using CCSD(T) predicts the EA to be 1.469 eV. Another calculation performed by Li *et al.* using the multi-configuration Dirac-Hartree-Fock method (MCDHF) gives a slightly lower estimate of 1.405 eV [7]. Older studies of varying quality estimate the EA to be in the range 1.2-1.9 eV [8][9]. With a possible experimental value of the EA in the next upcoming years, it is more topical than ever to perform new calculations with the aim to determine the EA of Po.

In this project, the MCDHF method combined with a relativistic configuration interaction (RCI) approach will be used to compute a new estimate of the EA. Unlike the previous estimate obtained with MCDHF, these calculations will be performed using a multi-reference and both the $6s$- and $6p$-orbital will be considered valence. The main correlation effects will be captured by allowing single and double substitutions from the valence orbitals. The effect on the EA will be studied when including triple substitutions for the negative ion in the additional RCI calculation.

2. Theory

This section starts with a review of the physics of negative ions and why Po is an interesting element to study. This is followed by a brief introduction to the theoretical framework necessary to understand the foundations of the many-electron atomic structure method used in this work. A motivation will be given to why it is necessary to use a relativistic approach when performing calculations on the EA of Po.

2.1. Negative ions

In the simplest way, a negative ion can be viewed as an atom that has gained an extra electron. However, the atomic structure of negative ions is considerably different and more complex if compared to neutral and positively charged ions. Due to the excess negative charge, the valence electrons do not experience a r^{-1} Coulomb potential at large distances. Instead, the extra electron will deform the electron cloud and polarize it, illustrated in fig. 1.

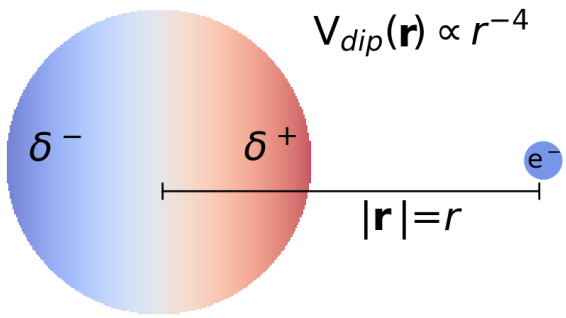

Figure 1: The figure illustrates how the additional electron polarizes the neutral atom. When the extra electron is introduced, the atomic charge will be redistributed and the dipolarization will be proportional to the electric field of the electron. The induced dipole will in turn give rise to an attractive potential $V_{\text{dip}}(\mathbf{r}) \propto r^{-4}$ which binds the extra electron to the atom. If the attraction is strong enough, a stable negative ion can be formed.

The induced dipole will result in a short range r^{-4} polarization potential $V_{\text{dip}}(\mathbf{r})$ which will attract the valence electrons. The relation between $V_{\text{dip}}(\mathbf{r})$ and the distance to the nucleus r can be derived by noting that the induced atomic dipole $\mathbf{p}$ will be proportional to the electric field $\mathbf{E}$ of the electron

$$\mathbf{p} = \alpha \mathbf{E} = \alpha \frac{e}{4\pi\epsilon_0 r^2} \hat{\mathbf{r}} \Rightarrow |\mathbf{p}| \propto \frac{1}{r^2}, \tag{1}$$

where the constant of proportionality α is called the atomic polarizability [10]. This

implies that the polarization potential $V_{\text{dip}}(\mathbf{r})$ arising from the induced dipole can be written as

$$V_{\text{dip}}(\mathbf{r}) = \frac{\mathbf{p} \cdot \hat{\mathbf{r}}}{4\pi\epsilon_0 r^2} \Rightarrow V_{\text{dip}}(\mathbf{r}) \propto \frac{1}{r^4}. \tag{2}$$

Due to the weak attractive potential, negative ions only have a finite number of bound states compared to positive ions where the number of states is infinite [2]. Most elements can form negative ions, however there are exceptions where the valence electrons are so weakly bound such that no stable anion naturally can exist. For example, the noble gases do not exist as negative ions due to their closed shell structure. The number of bound states also varies and it is common for a negative ion to only have one. Since the attractive potential which binds the extra electron to the system is a consequence of many-electron interaction, electron correlation is fundamental in the formation of stable negative ions. Therefore, negative ions are ideal candidates for investigating effects related to electron correlation. One important concept when studying negative ions is the electron affinity (EA). The electron affinity corresponds to the binding energy of the extra electron and can be viewed as a measurement of the correlation energy. For a neutral atom A and its negative counterpart A^- both in their respective groundstates, the electron affinity is defined as the difference between the total binding energies [11]

$$\text{EA} \equiv E_{\text{tot}}(\text{A}) - E_{\text{tot}}(\text{A}^-). \tag{3}$$

The relation between the EA and the energy levels of a neutral atom A and its anion A^- is illustrated in fig. 2.

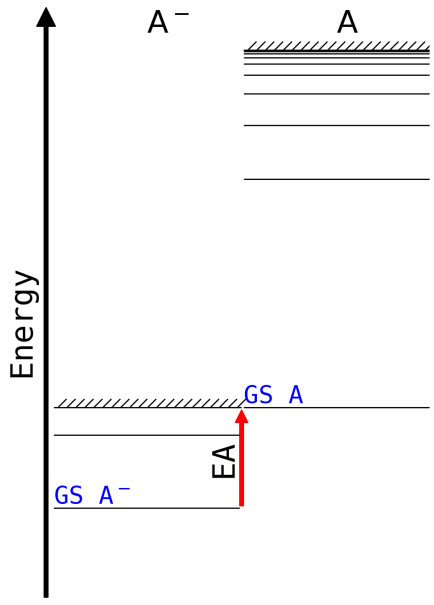

Figure 2: The diagram illustrates how the energy levels are typically distributed in a neutral atom A and its corresponding anion A^-. The EA is defined as being the difference in energy between the ground state of the anion A^- and the neutral atom A.

From an experimental point of view, not all negative ions are equally easy to investigate. In order to measure the electron affinity, one electron is photodetached from the anion and the energy threshold is determined. A general method for obtaining electron affinities is laser photodetachment spectroscopy, where a laser beam is overlapped with a beam of negative ions. The photon energy E_γ is scanned over the electron affinity threshold E_{EA} while the rate of neutral atoms resulting from photodetachment is measured as a function of the photon energy. The EA can be deduced by studying the onset of the production of neutral atoms [4]. For photons with energies $E_\gamma \geq E_{\mathrm{EA}}$ in the vicinity of the energy threshold, the photodetachment cross section σ is described by the Wigner threshold law [11]

$$\sigma \propto (E_\gamma - E_{\mathrm{EA}})^{l+1/2}. \tag{4}$$

Since photons carry an angular momentum of 1 (in atomic units with $\hbar = 1$), it is expected that the detached electron will have an angular momentum of $l = l_0 \pm 1$ where l_0 denotes the angular momentum of the electron as it was bound to the nucleus [2]. The Wigner law shows that the sharpest threshold for detachment will be when the outgoing electron has an angular momentum $l = 0$. The relation between the angular momentum of the outgoing electron and the sharpness of the threshold is illustrated in fig. 3.

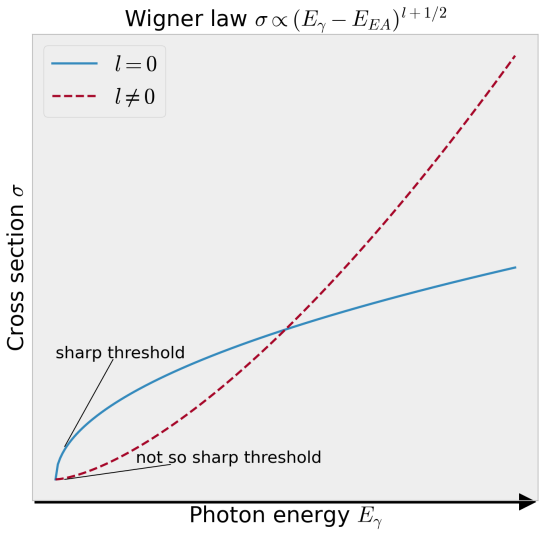

Figure 3: The solid curve corresponds to the photodetachment cross section obtained from the Wigner law when the outgoing electron has zero angular momentum $l = 0$. Similarly, the dashed curve represents the cross section when the outgoing electron has non-zero angular momentum $l \neq 0$. As can be viewed in the figure, the cross section is sharp when $l = 0$, indicating that the electron affinity can be determined with high accuracy if the outgoing electron has zero angular momentum.

If the valence electron is initially in a p-orbital, the outgoing electron can be described by two partial waves corresponding to an s-wave and a d-wave. However, due to a centrifugal force being present for $l > 0$, the outgoing d-wave will be suppressed [12].

Therefore, the most accurate measurements can be made for negative ions with valence electrons in p-orbitals.

In fig. 4, the accuracy with which the EA has been measured or calculated is plotted for the elements with known or predicted bound states of the corresponding anion. The data is taken from the actively maintained Wikipedia page "Electron affinity (data page)" (accessed in October 2022) [13]. From fig. 4, it is possible to conclude that in general, the accuracy is much better for the atomic ions with valance electrons in p-orbitals. In a recent study by Kristiansson *et al.*, the EA of oxygen was measured at the DESIREE facility at Stockholm university with a remarkable accuracy of $\sim 10^{-7}$ eV [4]. However, some of these elements display uncertain characteristics, where the most noticeable example is Po with the electron affinity 1.40(7). This value was obtained by Li *et al.* through computations made with MCDHF [7]. As it stands today, no experimental value of the EA exists for Po. Therefore, it is of great interest to get a measurement of the EA through experiment. Until then, a more accurate value must be obtained through computational methods.

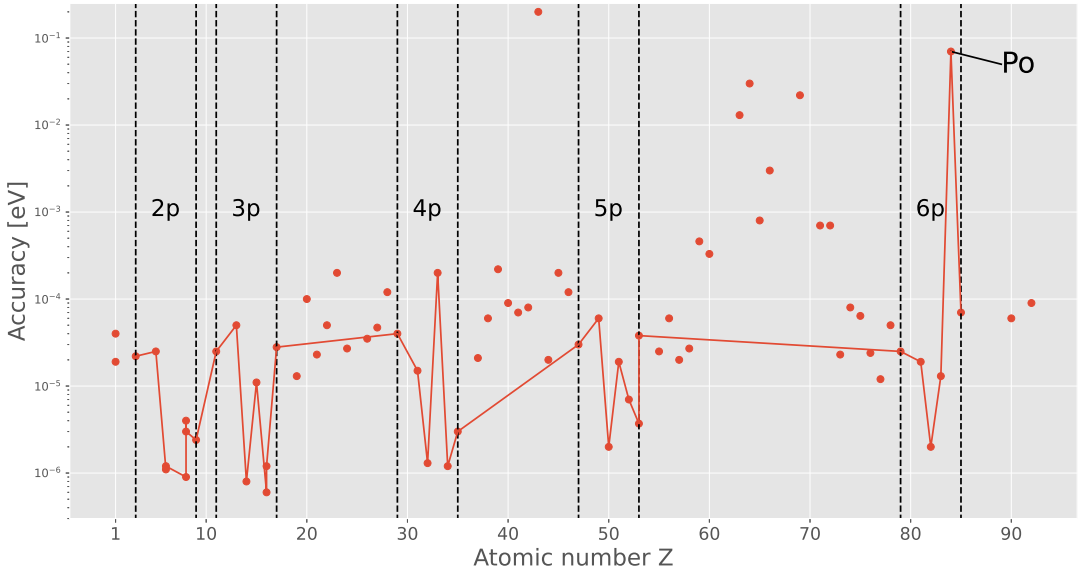

Figure 4: The graph display the accuracy in eV with which the electron affinity has been measured for bound anions up to U ($Z = 92$). For Po ($Z = 84$), the given value is from a calculation. The red line goes through all elements where the corresponding anion have valence electrons in p-orbitals.

2.2. The many-electron ion

A stationary state of an N-electron ion is described by its wave function $\Psi(\mathbf{q}_1,...,\mathbf{q}_N)$ where $\mathbf{q}_i = (\mathbf{r}_i,\sigma_i)$ denotes the spatial and spin coordinates for the i:th electron. The Born interpretation of the wave function states that the probability density function is

given by the square of the modulus $|\Psi|^2$. The energy E associated with a general atomic eigenstate is determined by solving the eigenvalue problem $\hat{H}\Psi = E\Psi$, where $\hat{H}$ is the Hamilton operator. For an N-electron system, the non-relativistic Hamiltonian can be expressed in the general form

$$\hat{H} = -\sum_{i=1}^{N}\left(\frac{h^2}{8\pi^2 m}\nabla_i^2 + \frac{Ze^2}{4\pi\epsilon_0 r_i}\right) + \frac{1}{2}\sum_{i\neq j}^{N}\frac{e^2}{4\pi\epsilon_0 r_{ij}}. \tag{5}$$

The first two terms is a sum of one-electron Hamiltonians given by the kinetic energy operator as well as the electron-nuclear Coulomb potential. The solution to each of the one-electron Hamiltonians are given by hydrogenic wave functions. The third term describes the Coulomb interaction between electrons i and j separated by the distance $r_{ij} = |\mathbf{r}_i - \mathbf{r}_j|$ [14].

When the third term is included, it is no longer possible to obtain an exact solution for the many-electron ion. By making a number of reasonable assumptions, it is however possible to find an approximate solution using a numerical approach. One of the most well known methods for this purpose is the Hartree-Fock (HF) approximation. In the Hartree-Fock model, it is assumed that the motion of the electrons is uncorrelated and that the total wave function Ψ can be represented as a product of single-electron spin-orbitals. These spin-orbitals are assumed to be separable into a spatial component $u(\mathbf{r})$ and a spin component $\chi(\sigma)$. If the electrons are modelled to be moving in a central field, the spatial component $u(\mathbf{r})$ can be further divided into a radial $P_{nl}(r)$ and an angular part $Y_{lm_l}(\theta,\varphi)$. Each orbital is defined by an unique set of quantum numbers $\{n, l, m_l, m_s\}$ and can be written as [15]

$$\phi(nlm_l m_s; \mathbf{q}) = \frac{1}{r}P_{nl}(r)Y_{lm_l}(\theta,\varphi)\chi_{m_s}(\sigma). \tag{6}$$

When Pauli's exclusion principle is taken into account, further restrictions are imposed on the electron wave function and it is required that the wave function is anti-symmetrical under the interchange of two electrons. One way of ensuring anti-symmetry is by constructing the wave function as a normalized Slater determinant

$$\Psi(PLS) = \frac{1}{\sqrt{N!}}\begin{vmatrix} \phi_{\alpha_1}(\mathbf{q}_1) & \phi_{\alpha_2}(\mathbf{q}_1) & \cdots & \phi_{\alpha_N}(\mathbf{q}_1) \\ \phi_{\alpha_1}(\mathbf{q}_2) & \phi_{\alpha_2}(\mathbf{q}_2) & \cdots & \phi_{\alpha_N}(\mathbf{q}_2) \\ \cdots & \cdots & \cdots & \cdots \\ \phi_{\alpha_1}(\mathbf{q}_N) & \phi_{\alpha_2}(\mathbf{q}_N) & \cdots & \phi_{\alpha_N}(\mathbf{q}_N) \end{vmatrix}. \tag{7}$$

For some LS-symmetries, it is necessary to use a linear combination of Slater determinants to construct wave functions that are eigenstates of the the non-relativistic Hamiltonian shown in eq. (5). These type of functions are referred to as configuration state functions (CSF). Each CSF is an eigenfunction of the orbital- and spin-angular momentum operators $\mathbf{L}^2$, L_z, $\mathbf{S}^2$, S_z as well as the parity operator Π [15]. It should be noted that CSF's can also be formed through explicit coupling and antisymmetrization for a given configuration by employing Racah algebra [16]. This is the approach used by the methods utilized in this work.

2.3. The Hartree-Fock equations

The Hartree-Fock equations are derived under the assumptions that the spin-orbitals are orthonormalized and that the wave function Ψ can be approximated with a single CSF. It is further assumed that the electrons are subject to a spherical symmetric potential. The latter is referred to as the central-field approximation. The main advantage of the central-field approximation is that only the radial part of the wave function has to be solved since the angular part will be given by spherical harmonics [15]. The many-electron Hamiltonian in eq. (5) can be viewed as consisting of a sum of one-electron operators as well as a sum of two-electron operators. Therefore, eq. (5) can be rewritten using the notation

$$H = \sum_{i=1}^{N} h(i) + \frac{1}{2}\sum_{i\neq j}^{N} g(i,j). \tag{8}$$

In atomic units, the two operators h_i and g_{ij} are given by

$$h(i) = -\frac{1}{2}\nabla_i^2 - \frac{Z}{r_i},\ g(i,j) = \frac{1}{r_{ij}}. \tag{9}$$

Since the electronic states building the wave function are assumed to be orthonormalized $\langle\phi_i|\phi_j\rangle = \delta_{ij}$, it is possible to apply the Slater-Condon rules to calculate the expectation value $\langle\Psi|H|\Psi\rangle$ and hence the energy E [17]. Note that this only applies to CSF's constructed as Slater determinants and not with Racah algebra. Because electrons with the same distribution are indistinguishable, the energy can be expressed in terms of a pair of arbitrary coordinates $(\mathbf{q},\mathbf{q}')$ making it possible to define $\hat{h} = h(\mathbf{r})$ and $\hat{g} = g(\mathbf{r},\mathbf{r}')$. Computing the expectation value yields the expression

$$E = \langle\Psi|H|\Psi\rangle = \sum_{i=1}^{N}\langle\phi_i|\hat{h}|\phi_i\rangle + \frac{1}{2}\sum_{i,j=1}^{N}\Big(\underbrace{\langle\phi_i\phi_j|\hat{g}|\phi_i\phi_j\rangle}_{J_{ij}} - \underbrace{\langle\phi_i\phi_j|\hat{g}|\phi_j\phi_i\rangle}_{K_{ij}}\Big). \tag{10}$$

The two integrals corresponding to an interaction between electrons are referred to as the Coulomb term J_{ij} and the exchange term K_{ij} [18]. The exchange interaction has no classical analogue and is a consequence of the required anti-symmetry of the wave function. In the notation used in eq. (10), it is implicitly understood that the first placeholder in each ket or bra is reserved for the coordinate $\mathbf{q}$ while the second is reserved for $\mathbf{q}'$, meaning for example that $|\phi_i\phi_j\rangle = |\phi_i(\mathbf{q})\phi_j(\mathbf{q}')\rangle$.

The variational principle states that the exact energy E_{exact} is less than or equal to the energy E obtained from an approximated wave function Ψ [18]. If Ψ is assumed to be normalized, this condition corresponds to

$$E = \langle\Psi|H|\Psi\rangle \geq E_{\text{exact}}. \tag{11}$$

Therefore, it is possible to approach the exact solution by choosing a wave function Ψ which minimizes the energy E where E_{exact} will be the lower bound to the approximated energy E. An approximate solution to the wave function can therefore be obtained by

varying the orbitals $\{\phi_i\}_{i=1}^N$ with the goal to minimize E. By introducing a set of Lagrange multipliers ε_{ij}, it is possible to include the constraint that the orthonormality of the orbitals must be preserved. This defines the Lagrangian

$$L = E - \sum_{i,j=1}^{N} \varepsilon_{ij}(\langle\phi_i|\phi_j\rangle - \delta_{ij}). \tag{12}$$

If a variation is applied to the Lagrangian and requiring that the first variation of L is set to zero, the following equation is obtained

$$\delta L = \sum_{i=1}^{N} \delta\langle\phi_i|\hat{h}|\phi_i\rangle + \frac{1}{2}\sum_{i,j=1}^{N}(\delta J_{ij} - \delta K_{ij}) - \sum_{i,j=1}^{N}\varepsilon_{ij}\delta\langle\phi_i|\phi_j\rangle = 0. \tag{13}$$

Without writing out the different steps explicitly, the various terms of eq. (13) can be simplified by using the hermiticity of the operators and the indistinguishability of electrons. Solving for an arbitrarily chosen orbital $\phi_i(\mathbf{q})$ yields the equation

$$\begin{aligned} h(\mathbf{r})\phi_i(\mathbf{q}) + \sum_{j=1}^{N}\left[\int d\mathbf{q}'\frac{|\phi_j(\mathbf{q}')|^2}{|\mathbf{r}-\mathbf{r}'|}\right]\phi_i(\mathbf{q}) \\ - \sum_{j=1}^{N}\left[\int d\mathbf{q}'\frac{1}{|\mathbf{r}-\mathbf{r}'|}\phi_j^*(\mathbf{q}')\phi_i(\mathbf{q}')\right]\phi_j(\mathbf{q}) = \varepsilon_i\phi_i(\mathbf{q}). \end{aligned} \tag{14}$$

The expression can be further simplified by using the fact that that the spin components fulfil $\chi(m_{s_i})\chi(m_{s_j}) = \delta_{ij}$ and thus eq. (14) can be expressed only as a function of the spatial component [17]

$$\begin{aligned} h(\mathbf{r})u_i(\mathbf{r}) + \sum_{j=1}^{N}\left[\int d\mathbf{r}'\frac{|u_j(\mathbf{r}')|^2}{|\mathbf{r}-\mathbf{r}'|}\right]u_i(\mathbf{r}) \\ - \sum_{j=1}^{N}\left[\delta(m_{s_i},m_{s_j})\int d\mathbf{r}'\frac{1}{|\mathbf{r}-\mathbf{r}'|}u_j^*(\mathbf{r}')u_i(\mathbf{r}')\right]u_j(\mathbf{r}) = \varepsilon_i u_i(\mathbf{r}). \end{aligned} \tag{15}$$

This is the Hartree-Fock equations on the non-canonical form where the Lagrange multiplier ε_i is the energy associated with the orbital ϕ_i. Since the integrals themselves are dependent on the orbitals, the equations must be solved iteratively. This is why solving the Hartree-Fock equations is commonly referred to as a self-consisted-field (SCF) procedure. The procedure can be summarized as follows.

1. Make an initial guess for the orbitals $\{\phi_i\}_{i=1}^N$.
2. Calculate the potentials.
3. Solve equation (15) keeping the potentials fixed.
4. Restart from step 2 with the new orbitals until convergence is obtained.

2.4. Multi-configuration Hartree-Fock

The energy E_{HF} obtained from calculations with the Hartree-Fock method is merely an approximation to the exact electronic energy E_{exact}. In the HF equations, the exchange interaction can be viewed as a form of spin-correlation between the electrons arising as a consequence of the anti-symmetry of the wave function. Apart from the spin-correlation, no additional electron correlation is considered in the HF method and the correlated motion of the electrons is completely neglected [15]. If electron correlation due to the Coulomb interaction is taken into account, the electrons will mutually repel which will decrease the energy of the system. Therefore, the exact energy can be viewed as a lower bound to E_{HF}. The deviation from the exact energy is defined as being the correlation energy [15, p. 67]

$$E_{\mathrm{corr}} = E_{\mathrm{exact}} - E_{\mathrm{HF}}. \tag{16}$$

When performing calculations on atomic structure, the aim is to reach an as accurate as possible approximation for the desired properties of the atom. It is thus in general preferable to introduce electron correlation in the calculations. Correlation can be included in the HF method by expressing the electronic wave function as a linear combination of CSF's rather than being represented by a single CSF. The eigenstate in a basis of CSF's is called an atomic state function (ASF). For a given parity P and LS-symmetry, the ASF can be written as [15, p. 73]

$$\Psi(\gamma PLS) = \sum_{i=1}^{M} c_i \Phi(\gamma_i PLS), \text{ where } \sum_{i=1}^{M} |c_i|^2 = 1. \tag{17}$$

In the above expression, $\Phi(\gamma_i PLS)$ denotes a single CSF with c_i being the expansion coefficient and γ_i representing other properties necessary to uniquely describe the CSF, such as the dominant electron configuration. The corresponding energy expression will be given by

$$E = \sum_{i=1}^{M} c_i^2 H_{ii} + 2 \sum_{i>j}^{M} c_i c_j H_{ij}. \tag{18}$$

The integrals H_{ij} are elements of a symmetric matrix referred to as the interaction matrix with elements defined as [15, p. 74]

$$H_{ij} = \langle \Phi(\gamma_i PLS) | H | \Phi(\gamma_j PLS) \rangle. \tag{19}$$

Solving the HF equations with a multi-configuration approach is similar to that of a single CSF. The HF equations will be extended to include integrals which account for the interaction between CSF's and not only exchange of electrons within a single CSF. The expansion coefficients are obtained through a configuration interaction (CI) calculation. The CI calculation corresponds to solving the eigenvalue problem

$$(\mathbf{H} - E_m \mathbf{I}) \mathbf{c}_m = 0. \tag{20}$$

In the above equation, $\mathbf{H}$ is the interaction matrix with elements given by eq. (19) and $\mathbf{I}$ is the identity matrix with the same dimension as $\mathbf{H}$. For an $M \times M$ matrix, there are in total M eigenstates. The state m has a corresponding eigenenergy E_m and an eigenvector $\mathbf{c}_m$ which contains the expansion coefficients for that particular state m [15].

2.5. Relativistic effects

Relativistic effects do influence the physics of all ions and atoms, but the significance of these effects will generally increase with the nuclear charge Z. If relativistic effects are considered, the electronic energy levels will be shifted and the atoms may display characteristics which were not predicted in the non-relativistic picture. A few common examples of atomic properties which are consequences of relativity include the yellow-like colours of Cu ($Z = 29$) and Au ($Z = 79$) and the low melting point of Hg ($Z = 80$) [19]. The dependency of relativistic effects on the nuclear charge Z can be investigated for hydrogen-like ions without using a fully relativistic treatment of the atom.

From the theory of special relativity, the observed mass of the electron will be dependent on its speed. In its own rest frame the electron has a mass denoted by m_e. But according to the equations of relativity, the observed mass m_{rel} will increase with the electron speed v according to [19]

$$m_{\text{rel}} = \frac{m_e}{\sqrt{1 - \frac{v^2}{c^2}}}. \tag{21}$$

The speed of the electron is dependent on the nuclear charge Z which can be examined with the Bohr model for hydrogen-like ions. In atomic units, the mean speed $\langle v \rangle$ of the electron can be expressed in terms of the principal quantum n and the nuclear charge Z

$$\langle v \rangle = \frac{Z}{n}. \tag{22}$$

Likewise, the mean radius $\langle r \rangle$ can be expressed in terms of the speed $\langle v \rangle$, nuclear charge Z and the mass m_{rel}

$$\langle r \rangle = \frac{Z}{m_{\text{rel}} \langle v \rangle^2}. \tag{23}$$

Since $\langle v \rangle \propto Z$ it is expected that m_{rel} will increase for heavier ions. Similarly, when both the speed $\langle v \rangle$ and the mass m_{rel} are increased, the radius $\langle r \rangle$ decrease and the inner atomic orbitals will be contracted. A contraction of the s- and p-orbitals will generally be observed since they have a large electron density close to the nucleus compared to orbitals with higher angular momentum l and thus higher velocity [19]. The contraction is said to be a direct relativistic effect. However, for orbitals with higher angular momentum l which are located farther away from the nucleus the opposite effect is expected and the orbitals are instead detracted. This is because the electron density is increased close to the nucleus when the inner orbitals are contracted thus the shielding becomes more effective and the outer electrons will experience a weaker interaction with the nucleus.

The detraction of the outer orbitals are said to be an indirect relativistic effect. This is illustrated in fig. 5 where the 5d- and 6s-orbitals for Po are plotted. A slight detraction of the 5d-orbital is observed while the 6s-orbital is significantly contracted.

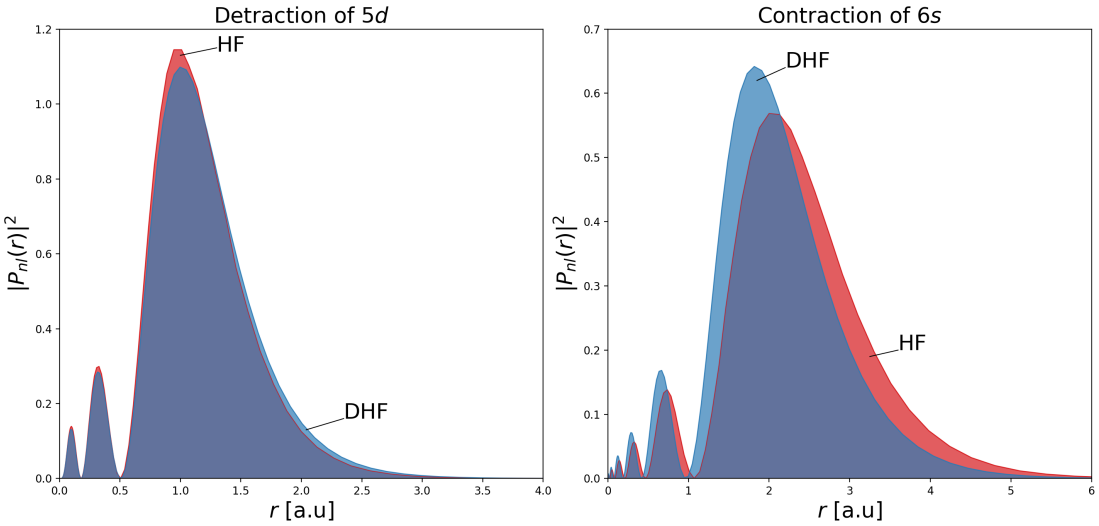

Figure 5: The detraction of the 5d-orbital and the contraction of the 6s-orbital for Po. The red orbitals marked with HF are from non-relativistic calculations while the blue orbitals marked with DHF are relativistic.

Another important relativistic effect is the spin-orbit coupling which gives rise to fine structure in atomic spectra. The spin-orbit coupling refers to the interaction between the spin of the electron with its motion around the nucleus. For an electron moving in a spherical potential, it can be shown through a semi-classical derivation that an extra term appears in the Hamiltonian which is given by [20]

$$H_{so} = \frac{1}{2}\alpha^2 \frac{Z}{r^3}\mathbf{L}\cdot\mathbf{S}. \tag{24}$$

The fine structure constant α is defined as $\alpha = e^2/(4\pi\varepsilon_0\hbar c) \approx 1/137$. The corresponding energy shift ΔE is determined by evaluating the integral $\langle\Psi|H_{so}|\Psi\rangle$,

$$\begin{aligned}\Delta E = \langle\Psi|H_{so}|\Psi\rangle &= \frac{Z}{2}\alpha^2\Big\langle\frac{1}{r^3}\Big\rangle\langle\mathbf{L}\cdot\mathbf{S}\rangle = \frac{Z}{2}\alpha^2\Big\langle\frac{1}{r^3}\Big\rangle\frac{1}{2}\langle\mathbf{J}^2-\mathbf{L}^2-\mathbf{S}^2\rangle \\ &= \frac{Z}{4}\alpha^2\Big\langle\frac{1}{r^3}\Big\rangle\left[j(j+1)-l(l+1)-s(s+1)\right].\end{aligned} \tag{25}$$

When evaluating $\langle r^{-3}\rangle$, it is only necessary to consider the radial part of the wave function $P_{nl}(r)$ (technically, R_{nl} is the radial part with $rR_{nl} = P_{nl}$). Since the electron is moving in a spherical Coulomb potential, $P_{nl}(r)$ will fulfil the radial equation,

$$P''_{nl} = \left[\frac{l(l+1)}{r^2} - \frac{2Z}{a_0 r} + \frac{Z^2}{n^2 a_0^2}\right]P_{nl}. \tag{26}$$

The above equation can be used to derive a relationship which is useful when calculating expectation values $\langle r^s \rangle$ for integer values of s. The derivation is left out of this text, but can be viewed in appendix A. After evaluating $\langle r^{-3} \rangle$ in atomic units with $a_0 = 1$, the energy shift will be equal to [20]

$$\Delta E = \frac{Z^4 \alpha^2}{4l(l+\frac{1}{2})(l+1)n^3} \left[j(j+1) - l(l+1) - s(s+1) \right]. \tag{27}$$

From the above expression follows that $\Delta E \propto Z^4$ and therefore, for sufficiently heavy ions, the spin-orbit coupling will compete with the Coulomb interaction. Even though the relationship $\Delta E \propto Z^4$ was explicitly derived for hydrogenic ions, the same relationship is observed for atoms and ions in general [17]. The strong dependence on Z for the spin-orbit coupling can be illustrated by studying the magnitude of the fine structure splitting. In fig. 6, the experimental values for the fine structure of the three lightest elements with the outer electron configuration ns^2np^4 are viewed [21]. From this diagram, it is observed that with increasing Z, the energy splitting between levels with different values of the total angular momentum J becomes significantly larger. This is an immediate consequence of the Z-dependence of the spin-orbit coupling.

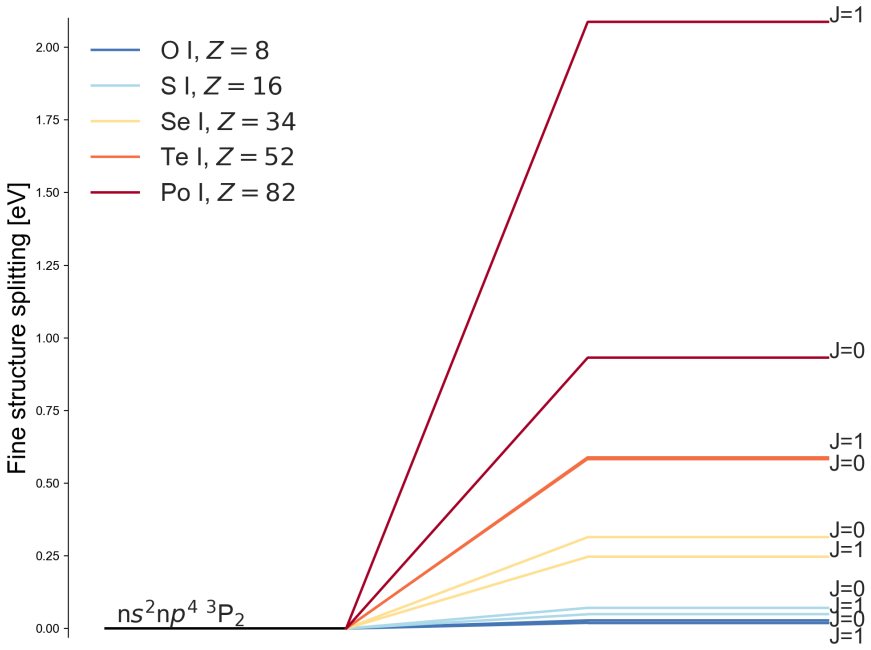

Figure 6: The fine structure splitting for the ground state configuration $ns^2np^4\ ^3\mathrm{P}$ of O I, S I, Se I, Te I and Po I. It is apparent that the energy splitting between two levels with different values for J is larger for higher Z.

Both with respect to the relativistic mass and the spin-orbit coupling, it is evident that the non-relativistic treatment of the electron is more problematic for heavily charged ions. Relativistic effects are accounted for in the covariant Dirac equation. However,

solving the Dirac equation for a multi-body system is complicated. In the Breit-Pauli approximation, some relativistic effects are accounted for while still treating the radial orbitals non-relativistic. This is accomplished by expanding the relativistic many-electron equation and including terms of order α^2 to the non-relativistic Hamiltonian in eq. (5) as corrections to the Dirac-Coloumb-Hamiltonian [15, p. 129].

2.6. Multi-configuration Dirac-Hartree-Fock

It is possible to extend the MCHF calculations to include some relativistic corrections through the Breit-Pauli approximation. A more thorough alternative is to use the fully relativistic multi-configuration Dirac-Hartree-Fock (MCDHF) method, which is implemented in the code package `GRASP2018` [22]. To perform the SCF calculation, the Dirac-Coulomb Hamiltonian H_{DC} is used. Similarly as with the non-relativistic Hartree-Fock method, the H_{DC} will consist of an one-electron and a two-electron part. According to Dirac's theory, the one-electron operator will consist of the kinetic energy operator T_i and a nuclear potential $V_{\text{nuc}}(r_i)$ from an extended charge distribution. The one-electron operator h_i is given by

$$h_i = T_i + V_{\text{nuc}}(r_i) = c\boldsymbol{\alpha}_i \cdot \boldsymbol{p}_i + (\beta_i - 1)c^2 + V_{\text{nuc}}(r_i), \tag{28}$$

where c is the speed of light, $\boldsymbol{\alpha}_i$ and β_i are the 4×4 Dirac matrices for electron i and $\boldsymbol{p}_i$ is the electron angular momentum operator $-i\nabla_i$ [23]. As a first approximation, the two-electron interaction can be assumed to only consist of the Coulomb interaction

$$h_{ij} = \frac{1}{r_{ij}}. \tag{29}$$

Combining the different parts gives the full Dirac-Coulomb Hamiltonian H_{DC} for an N-electron system [23]

$$H_{DC} = \sum_{i=1}^{N} \left[c\boldsymbol{\alpha}_i \cdot \boldsymbol{p}_i + (\beta_i - 1)c^2 + V_{\text{nuc}}(r_i) \right] + \sum_{i<j}^{N} \frac{1}{r_{ij}}. \tag{30}$$

In a relativistic framework, the two-electron interaction is much more complex. The leading correction to the Coulomb interaction is called the transverse photon interaction which in the low frequency limit $\omega_{ij} \to 0$ will reduce to the Breit interaction [19]

$$h_{ij}^{\text{Breit}} = -\sum_{i<j}^{N} \frac{1}{2r_{ij}} \left[(\boldsymbol{\alpha}_i \cdot \boldsymbol{\alpha}_j) + \frac{(\boldsymbol{\alpha}_i \cdot \mathbf{r}_{ij})(\boldsymbol{\alpha}_j \cdot \mathbf{r}_{ij})}{r_{ij}^2} \right]. \tag{31}$$

It is also possible to expand the Hamiltonian to include additional QED corrections such as self energy (SE) and vacuum polarization (VP). In its full form, the Hamiltonian can be written as $H = H_{DC} + H_{Breit} + H_{SE} + H_{VP}$. The Breit and QED contributions are included by performing a final diagonalization of the extended Hamiltonian H in a relativistic configuration interaction (RCI) calculation with an orbital basis determined

in the initial MCDHF procedure. The effect on the binding energy of the ground state of Po when the Breit interaction and the leading QED corrections are accounted for in the RCI calculation is illustrated in fig. 7.

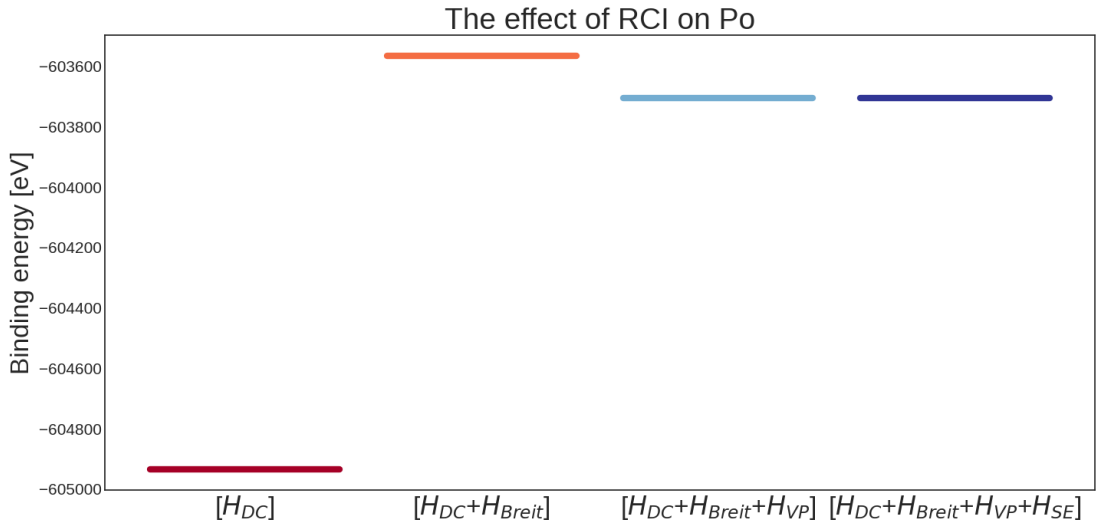

Figure 7: The effect on the binding energy for the ground state of Po when expanding the Hamiltonian to include the Breit interaction and the leading QED corrections. The calculation was performed with a single CSF representing the ground state, i.e. a DHF model without electron correlation effects.

The wave function Ψ is described by an ASF characterized by its parity P and the total angular momentum J. The ASF $\Psi(\gamma PJ)$ is expressed as a linear combination of CSF's $\Phi(\gamma_i PJ)$ and expansion coefficients c_i [22]

$$\Psi(\gamma PJ) = \sum_{i=1}^{N_{CSF}} c_i \Phi(\gamma_i PJ). \tag{32}$$

The parameters γ_i represent other necessary properties to fully describe the CSF's, such as orbital occupancy. Each CSF is represented as a sum of anti-symmetric products of orthonormal one-electron Dirac 4-spinors [22]

$$\phi_{n\kappa m}(\mathbf{q}) = \frac{1}{r} \begin{pmatrix} P_{n\kappa}(r)\chi_{\kappa m}(\theta,\varphi) \\ iQ_{n\kappa}(r)\chi_{-\kappa m}(\theta,\varphi), \end{pmatrix} \tag{33}$$

where n is the principal quantum number, and κ and m are the relativistic angular quantum number and its z-component respectively. $P_{n\kappa}(r)$ and $Q_{n\kappa}(r)$ represent the large and the small component of the radial wave function for the orbital $\phi_{n\kappa m}$, respectively. It can be shown that the large component will have $(n - l - 1)$ number of nodes [19, p. 41]. The H_{DC} do not commute with the $\mathbf{L}$ and $\mathbf{S}$ operators. Instead, the CSF's must satisfy [23]

$$\begin{aligned} &\Pi\Phi = P\Phi,\ P = (-1)^{l_1+\ldots+l_N}, \\ &\mathbf{J}^2\Phi = J(J+1)\Phi, \\ &J_z\Phi = M\Phi,\ M = -J, -J+1,\ldots,J. \end{aligned} \tag{34}$$

Both the expansion coefficients c_i and the one-electron orbitals are obtained through the SCF procedure of the MCDHF method. In the subsequent RCI calculation, the orbitals building the CSF's are kept fixed while the expansion coefficients are recalculated with an expanded Hamiltonian, as described earlier, to include the Breit interaction and leading QED effects. When doing calculations with `GRASP2018`, both a configuration multi-reference (MR) and an active set of orbitals $\{\phi_k\}$ (AS) are defined. Substitutions are allowed from the configurations within the MR to orbitals defined by the AS. By successively expanding the AS, it is therefore possible to add more layers of correlation. This corresponds to extending the CSF basis representing the ASF (32).

3. Method

The purpose of this section is to give a more detailed explanation to how the calculations were planned and performed. Different types of correlation effects are discussed and a motivation to why certain effects were included in the model is given. Some difficulties with performing calculations of the EA of Po are also discussed and possible approaches to handle these obstacles are presented.

3.1. The general procedure

The aim of the project was to compute a new estimate of the electron affinity of Po using the MCDHF method as implemented in the `GRASP2018` code. These calculations were combined with relativistic configuration interaction to include additional correlation effects as well as the Breit interaction and QED effects. The average energy of the full term of the ground state configuration of Po and Po^- was minimized in the SCF procedure. The states which are optimized are referred to as the target states which for Po are $[Xe]4f^{14}5d^{10}6s^26p^4\ {}^3P$ with $J = 0, 1, 2$ and for Po^- are $[Xe]4f^{14}5d^{10}6s^26p^5\ {}^2P^o$ with $J = 1/2, 3/2$.

Before carrying out the actual calculations of the EA, it was important to first construct a valid model in which correlation could be included in a structured manner. To begin with, the core and valence orbitals had to be defined. An appropriate multi-reference was also needed in order to include higher order correlation effects in the calculations. To make these decisions, initial estimates of the energies and the orbital wave functions were calculated. These first approximations were later improved by successively introducing correlation in the MCDHF+RCI procedure. The necessary steps required to perform a calculation using MCDHF and RCI implemented in `GRASP2018` are summarized in the flowchart displayed in fig. 8.

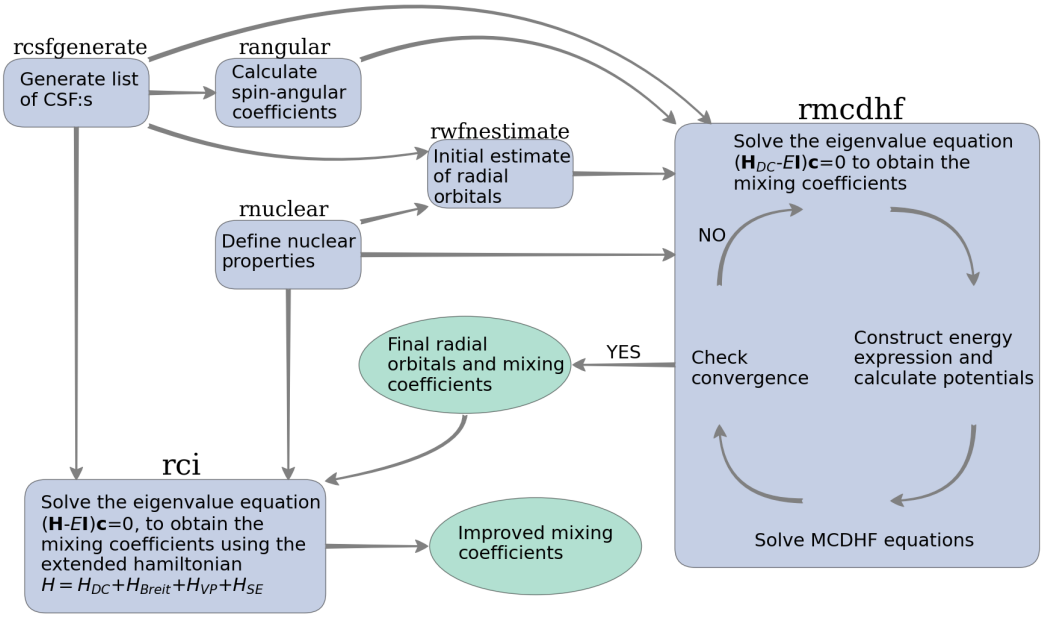

Figure 8: The flowchart illustrates the necessary components of a calculation with `GRASP2018` where each blue box represents a specific subroutine. Initially, the nuclear properties are defined with `rnuclear` and a list of CSF's is generated with `rcsfgenerate`. The spin-angular coeffcients are obtained from `rangular` and an initial guess for the radial orbitals are calcultaed in `rwfnestimate`. There is also an option in `rwfnestimate` to input a wave function file from previous runs. The new orbitals are optimized in `rmcdhf` in the SCF-procedure. Based on the orbital wave functions and the mixing coefficients obtained from `rmcdhf`, `rci` can be run to improve the wave function with an additional RCI calculation.

3.2. Adding correlation

Correlation is added to the model by extending the single-CSF representation of the HF/DHF wave function to a multi-CSF description as in eq. (32). The CSF's are generated by making electron substitutions from the reference configurations within an active set of orbitals. Since the Hamiltonian is a two-body operator at most, it is generally enough to consider single (S) and double (D) substitutions from the reference configurations. Higher order effects can be captured by extending the set of spectroscopic reference configurations to a multi-reference (MR) with additional strongly interacting configurations. In other words, the MR should consist of CSF's with large interactions with the target states of interest- which in our case are the ground terms of Po and Po^-. Assuming that the zero-order wave function only consist of the leading CSF ϕ_0 for some interaction H, the expansion coefficient for the CSF denoted ϕ_n can be estimated to first order by [19, p. 59]

$$c_n \approx \frac{\langle \phi_n | H | \phi_0 \rangle}{E_0 - E_n}. \tag{35}$$

The numerator, and hence c_n, will be large if the orbitals of the two different CSF's are occupying roughly the same region of space. Therefore, one possible way of identifying a suitable MR is based on the value of the expansion coefficients in the initial calculations performed with the target state as a single reference.

After a suitable MR is found, the active space of orbitals is successively expanded by adding new correlation orbitals. Correlation orbitals are typically not required to have the expected number of nodes. In this work, only the orbitals found in the target states were required to be spectroscopic and thus have the expected number of $(n-l-1)$ nodes. The MCDHF calculations were carried out in a layer-by-layer procedure where in each step, one new orbital per l-symmetry was added and only the newly added correlation orbitals were optimized. If more than one new orbital per l-symmetry is included at a time, issues with convergence are likely to occur in the SCF minimization.

The type of correlation considered decides which CSF's are included in the ASF in eq. (32). Three kinds of correlation effects can be defined if two electrons in the physical orbitals ab are substituted with the correlation orbitals $\alpha\beta$ in the replacement $ab \rightarrow \alpha\beta$ [15, p. 71].

1. If both ab are valence orbitals, the replacement represents valence-valence correlation (VVC).

2. If either a or b is a core orbital and the other one is a valence orbital, the replacement represents core-valence correlation (CVC).

3. If both orbitals ab are core orbitals, the replacement represent core-core correlation (CCC).

When optimizing the orbitals, only SD substitutions and VVC were considered. After the SCF procedure, the expansion coefficients were recalculated in an additional RCI calculation to include the Breit interaction and leading QED effects. After each new layer, the EA was calculated and compared to the values retrieved from the previous steps. This procedure was repeated until the EA had reached a satisfactory degree of convergence.

3.3. Effects from core-valence-correlation

Substitutions from core orbitals were not allowed in the SCF procedure since otherwise the size of the calculations would be too large. Instead, effects from CVC were investigated by extending the list of CSF's in a subsequent RCI calculation. CCC was not considered in this project at all. Typically, recalculating the spin angular coefficients

with `rangular` and reoptimizing the orbitals with `rmcdhf` is a much more time consuming process than running `rci`, which can be considered as just one iteration of the SCF procedure. By only running `rci`, effects from CVC will be included in the model while the computational time will be manageable.

3.4. Balancing correlation

The existence of negative ions is very much dependent on the ability of the extra electron to share the attractive field of the nucleus with the other electrons. The correlated motion of the electrons will result in a polarization of the electron cloud which will act as the attractive potential that binds the valence electrons to the system. Therefore, a more accurate approximation for the binding energy of the neutral atom will be obtained with less correlation compared to the anion. As mentioned above, a layer-by-layer method was employed in this work in which new correlation orbitals are added to the model in steps. Due to the anion being more dependent on correlation, the EA will tend to be underestimated if the binding energies used for Po and Po^- when calculating the EA are from the same step. A typical approach to adjust for this effect is to compare the value of the binding energy for the anion obtained from step x with value obtained for the neutral atom from step $(x-1)$. In this report, electron affinities obtained through this approach will be denoted with $\Delta x = 1$ while electron affinities computed from the same step will be denoted with $\Delta x = 0$.

More intricate ways of balancing correlation can be modelled within the actual calculations. For example, by including a larger set of orbitals in the active set for the anion, correlation effects are better balanced and a more representative value of the EA can be obtained [24]. Li *et al.* used another approach when calculating the EA by allowing SD substitutions for the neutral atom, but for the anion also include some triple (T) substitutions [7]. Inspired by the latter approach, which was carried out with MCDHF calculations, a procedure was constructed where extra correlation was added in the model of the anion Po^- through an additional RCI calculation where the list of CSF's is expanded to include SDT substitutions within a fixed active set. The model with only SD substitutions for both Po and Po^- will be referred to as SD-SD and the new model with SDT substitutions for Po^- will be referred to as SD-SDT.

To compare the convergence of the EA from the SD-SD and the SD-SDT model, a simple exponential function was fitted to the datapoints with the parameters A,B,C according to

$$f(x) = Ae^{-Bx} + C. \tag{36}$$

The value of C should be interpreted as being the total binding energy to which the calculations are converging to, while A can be thought of as representing the total error between the first data point and the estimated total binding energy. The value of B can be used as an indication of how fast the binding energy is converging as more correlation orbitals are included.

3.5. Handling large expansions with perturbation theory

Working with `GRASP2018` is to a large extent a matter of weighing the amount of correlation included against the computational cost. For example, the number of matrix elements evaluated in the configuration interaction with `rci` will scale as M^2 where M is the number of CSF's. For larger systems such as Po, the number of CSF's generated can be huge and it is therefore necessary to find ways to manage the large expansion. The SCF procedure is even more time consuming than the additional RCI calculation and determining the time it takes for the solution to reach self-consistency is hard to predict. Therefore it may be necessary to use methods to reduce the size of the calculations.

In `GRASP2018`, Brillouin-Wigner perturbation theory is implemented through a number of add-on programs and can be used to manage large expansions [19]. Using this method, the CSF's in the expansion are divided in to a zero-order and first-order space for each J symmetry. Each J-block of the interaction matrix can then be arranged on the following form

$$\begin{pmatrix} H^{00} & H^{01} \\ H^{10} & H^{11} \end{pmatrix}. \tag{37}$$

All matrix elements involving the zero-order space H^{00}, H^{10} and H^{01} are evaluated, but only the diagonal elements of H^{11} are computed [22]. In this manner, it is possible to reduce the amount of computations and improve the run times. This approach was used when adding the correlation layers VV2 and VV3. The zero-order spaces were determined by looking at the sizes of the expansion coefficients from the previous layer of correlation. It was decided that the CSF's corresponding to 99.99% of the wave function for each J-symmetry of a given MCDHF step was large enough to define the zero-order space in the next correlation layer.

3.6. HPC cluster calculations

For the last valence-valence layer and the core-valence layer, the computations were performed on the computer cluster Vera at C3SE at Chalmers. C3SE is one out of six high performance computing (HPC) centres in Sweden organised under NAISS [25]. Vera runs two types of CPU's, one with 32 cores and the other one with 64 cores. The `GRASP2018` package offers MPI versions of the most time consuming programs which makes it possible to employ parallel processing to reduce the run times. Therefore, the number of parallel processes were limited to 64 (hyperthreading is not allowed at Vera). Vera runs the SLURM workload manager which is a batch queuing software. To have your codes run, it is necessary to write a batch script where certain parameters are specified, such as estimated run time and the number of parallel processes. The script is queued and when a node meeting the requirements is available, the codes will be run and the results will be written to a directory of choice. An example of a batch script used for the core-valence layer of Po^- is found in appendix B.

4. Model

The main purpose of this section is to present the results from the preparatory calculations performed to define a suitable atomic structure model for Po and Po^-. These calculations are categorized in to three subsections. In the first part, results from the non-relativistic HF are compared to the corresponding values from relativistic DHF. These calculations were carried out to obtain bases for the orbital wave functions and to verify the need for a relativistic approach. The second subsection serves to motivate why the $6s$- and $6p$-orbitals should be considered belonging to the valence shell. In the third and final part, the approach that was used to decide which configurations to include in the MR for Po and Po^- is explained.

4.1. Initial estimate of EA

An initial calculation with the non-relativistic HF was performed to determine whether or not Po^- was bound in the independent particle model without electron correlation. By optimizing on the ground state for both Po and Po^- and comparing the total binding energies, Po^- was indeed found to be bound. The non-relativistic wave functions from HF were transformed to relativistic by using the built-in program `rwfnmchfmcdf`. These wave functions were used as initial estimates for the orbitals when the corresponding energies were calculated with MCDHF using a single-reference and without any additional correlation. The energy estimates for Po and Po^- were obtained by optimizing on the full terms and requiring that all orbitals should be physical. The first correlation layer consisting of the orbitals $\{7s,7p,6d,5f,5g\}$ was added to the AS and SD substitutions were allowed from the $6s$- and $6p$-orbitals. The binding energies and the corresponding EA for each step are viewed in table 1. When comparing the values in table 1, a significant decrease in the binding energy is observed for both Po and Po^- when using a relativistic approach.

Table 1: Initial estimates of the total binding energies and the electron affinity of Po using the ground state configuration of Po and Po^- as a single reference. The ΔHF values correspond to the difference of the total binding energy when compared to the initial calculation with HF.

	Po		Po^-		EA [eV]
Step	E [eV]	ΔHF [eV]	E [eV]	ΔHF [eV]	$\Delta x = 0$
HF	-562636.2527		-562637.4850		1.23230
HF+BP	-596870.4493	-34234.1966	-596871.4660	-34233.9810	1.01666
DHF	-604934.6648	-42298.4121	-604935.1957	-42297.7107	0.53084
DHF+RCI	-603705.2744	-41069.0217	-603705.8103	-41068.3253	0.53591
AS1	-604937.1466	-42300.8939	-604938.2273	-42300.7423	1.08075

4.2. Electron correlation: valence orbitals

Which of the orbitals should be treated as core or valence orbitals had to be determined. By computing the one-electron energy E_{nl} and the mean radii $\langle r \rangle$ of the six outermost orbitals, it was possible to identify which orbitals should be considered as valence orbitals. The radial probability density functions $|P_{nl}|^2$ were also plotted for the orbitals to get a qualitative measure of the overlap between the orbital wave functions. The computations were performed both with the non-relativistic HF and with DHF. By comparing the results from HF with the results computed with DHF, it was possible to investigate the effects of a relativistic treatment of the system. The energies and radial distances computed with HF are viewed in table 2, while the corresponding results from DHF are viewed in table 3. Since DHF is a relativistic approach, separate values for the one-electron energies will be obtained for orbitals with $l > 0$ depending on the total angular momentum $j = l \pm 1/2$. In table 3, the negative suffix corresponds to $j = (l - 1/2)$ and the positive to $j = (l + 1/2)$.

Table 2: The one-electron energies E_{nl} and the radial expectation values $\langle r \rangle$ for the outer orbitals $\{4f, 5s, 5p, 5d, 6s, 6p\}$ computed with HF.

	Po		Po^-	
	E_{nl} [a.u.]	$\langle r \rangle$ [a.u.]	E_{nl} [a.u.]	$\langle r \rangle$ [a.u.]
$4f$	8.2807105	0.41909	16.0585038	0.41909
$5s$	5.9621017	0.90602	11.4204909	0.90607
$5p$	4.40014835	0.96480	8.2977137	0.96484
$5d$	1.75530275	1.15067	3.0077746	1.15139
$6s$	0.6582527	2.39077	0.8574405	2.46226
$6p$	0.3414654	2.88500	0.1868595	3.16167

Table 3: The one-electron energies E_{nl} and the radial expectation values $\langle r \rangle$ for the outer orbitals $\{4f, 5s, 5p, 5d, 6s, 6p\}$ computed with DHF.

	Po		Po^-	
	E_{nl} [a.u.]	$\langle r \rangle$ [a.u.]	E_{nl} [a.u.]	$\langle r \rangle$ [a.u.]
$4f^-$	7.4950167971	0.424725	7.2494023201	0.424723
$4f^+$	7.2684202598	0.430550	7.0229051911	0.430549
$5s$	7.2327560112	0.818050	6.9870240136	0.818049
$5p^-$	5.3844631770	0.868195	5.1380959235	0.868239
$5p^+$	4.3566561310	0.951000	4.1114775965	0.950892
$5d^-$	1.6385988425	1.14841	1.3920871568	1.14849
$5d^+$	1.5015116054	1.18569	1.2558478086	1.18706
$6s$	0.80413535306	2.12118	0.57147995235	2.16521
$6p^-$	0.40295189829	2.56648	0.16027027146	2.70184
$6p^+$	0.30434578830	2.93946	0.061345112675	3.32871

The mean radii $\langle r \rangle$ of the outer orbitals are plotted in fig. 9. As expected for the relativistic calculations, the s-orbitals were contracted while the d- and f-orbitals were slightly shifted away from the nucleus. Similarly, the $5p$-orbital was contracted while the $6p$-orbital was detracted. This is due to the nucleus being more effectively shielded for electrons in the $6p$-orbital compared to electrons in the $5p$-orbital. It is also evident from fig. 9 that the valence electrons in the negative ion experience a weaker attraction to the nucleus compared to the neutral atom. The mean radii $\langle r \rangle$ for the $6s$- and $6p$-orbitals are noticeable larger for the anion, which indicates that the valence electrons are more tightly bound in the neutral atom. No significant difference in $\langle r \rangle$ is observed for the orbitals with $n = 4,5$.

The radial probability density functions $|P_{nl}|^2$ obtained with DHF for the six outermost orbitals are plotted in fig. 10. From these plots, it is evident that the $6s$- and $6p$-orbitals share the same region of space to a much larger extent if compared to the orbitals with $n = 4,5$. Based on the combined results presented above, it was decided to only treat the $6s$- and $6p$-orbitals as valence.

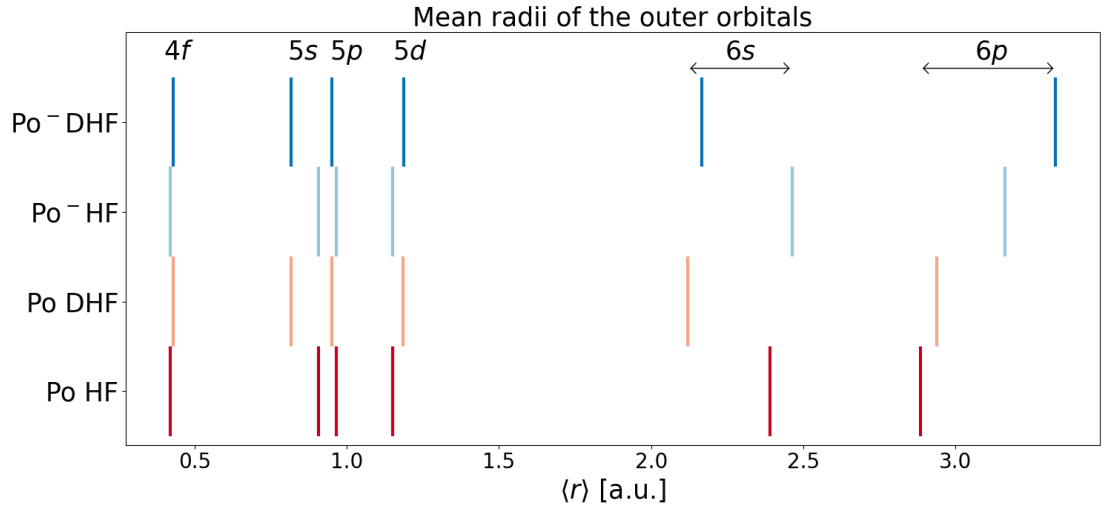

Figure 9: The mean radii $\langle r \rangle$ of the outer orbitals $\{4f^+, 5s, 5p^+, 5d^+, 6s, 6p^+\}$ computed with HF and DHF, respectively.

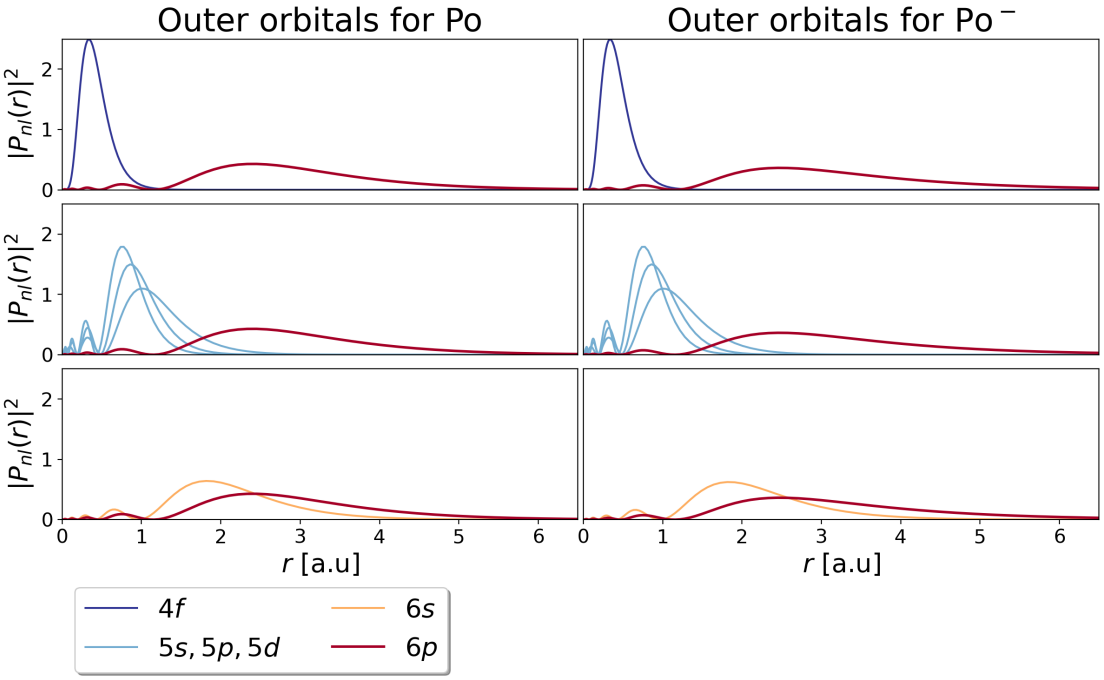

Figure 10: The curves correspond to the probability density $|P_{nl}(r)|^2$ for the outer orbitals $\{4f^+, 5s, 5p^+, 5d^+, 6s, 6p^+\}$ computed using DHF with the ground state configuration as a single reference. The red curve represent the $6p$-orbital and by comparing the plots, it is apparent that the $6s$-orbital has the most significant overlap with the $6p$-orbital.

4.3. Electron correlation: multi-reference

The MR should consist of configurations which have a significant interaction with the target state. One way of identifying the configurations which are the most correlated is through Z-dependent perturbation theory. By treating the electron-electron Coulomb interaction V_{ee} as a small perturbation to the one-electron Hamiltonian H_0 and expanding with respect to Z^{-1} gives a perturbed Hamiltonian H

$$H = Z^2(H_0 + \frac{1}{Z}V_{ee}). \tag{38}$$

It is possible to show that the zero-order energy is given as a sum of the hydrogenic energies of the electrons [15, p.69]

$$E_0 = -\frac{1}{2}\sum_{i=1}^{N}\frac{1}{n_i^2}. \tag{39}$$

Since E_0 is independent of the spin and angular momentum, it follows that E_0 is degenerate with respect to the CSF's with the same set of the quantum numbers n while preserving the total parity. According to results from first-order perturbation theory of degenerate states, the corresponding zero-order wave function ψ_0 can be expressed as a linear combination of the individual degenerate CSF's [26, pp. 300−303]. The set of configurations represented in ψ_0 is referred to as the Layzer complex [15, p. 69]. The configurations in the Layzer complex for Po and Po^- are displayed in table 4. In this table, only SD substitutions from the valance orbitals $6s$ and $6p$ up to the orbital $6f$ were considered.

Extending the MR to include the full Layzer complex would be too expensive. Therefore, it was necessary to identify which of these configurations were interacting the most strongly with the target state. To determine the interaction between the configurations, the AS was extended with the correlation orbitals $\{7s, 7p, 6d, 5f, 6f, 5g\}$ while using the ground state configuration as a single reference. A new list of CSF's was generated by allowing SD substitutions from the valance orbitals $6s$ and $6p$. From the sizes of the mixing coefficients c_i, it was possible to determine the contribution from the individual configurations to the total wave function. Configurations with values of $|c_i|^2$ in the range 0.25% to 0.81% are displayed in table 5. By weighing the computational cost against the accuracy of the calculations, it was decided to include configurations in the MR with mixing coefficients exceeding $|c_i|^2 = 0.36\%$. All of the configurations with mixing coefficients exceeding $|c_i|^2 = 0.36\%$ are found within the complex in table 4, except for the $6f$-orbital being interchanged with the $5f$-orbital.

Table 4: The configurations belonging to the Layzer complex of Po and Po^-, respectively. Only configurations that can be obtained through SD substitutions up to and including the $6f$-orbital are listed.

	Layzer complex
Po	$6s^26p^4$, $6s^26p^36f$, $6s6p^46d$, $6s^26p^26d^2$, $6p^6$, $6s^26p^26f^2$, $6p^46d^2$, $6p^46f^2$, $6s6p^36d6f$
Po^-	$6s^26p^5$, $6s^26p^46f$, $6s6p^56d$, $6s^26p^36d^2$, $6s^26p^36f^2$, $6p^56d^2$, $6p^56f^2$, $6s6p^46d6f$

Table 5: The configurations listed in each row are those who have an expansion coefficient greater or equal to a given value of c_i. The configurations are generated by allowing substitutions from the ground state configuration to the correlation orbitals $\{7s, 7p, 6d, 5f, 6f, 5g\}$.

c_i	$\lvert c_i\rvert^2$ [%]	Po	Po^-
0.09	0.81%	$6s^26p^4$, $6s6p^46d$	$6s^26p^5$
0.08	0.64%	$6s^26p^4$, $6s6p^46d$	$6s^26p^5$ $6s^26p^36d^2$ $6s6p^56d$
0.07	0.49%	$6s^26p^4$ $6s6p^46d$ $6s^26p^26d^2$,$5f6s^26p^3$	$6s^26p^5$ $6s^26p^36d^2$ $6s6p^56d$ $5f6s^26p^4$
0.06	0.36%	$6s^26p^4$ $6s6p^46d$ $6s^26p^26d^2$,$5f6s^26p^3$	$6s^26p^5$ $6s^26p^36d^2$ $6s6p^56d$ $5f6s^26p^4$
0.05	0.25%	$6s^26p^4$, $6s6p^46d$ $6s^26p^26d^2$, $5f6s^26p^3$	$6s^26p^5$, $6s^26p^36d^2$ $6s6p^56d$, $5f6s^26p^4$ $6s^26p^37p^2$

5. Results

In this section the most important results are presented. The results are primarily presented in eV and the conversion factor from a.u. to eV was defined as 1 a.u. = 27.211386245988 eV [27]. This section begins with presenting the binding energies and the EA obtained from the SD-SD model. After that, the corresponding results are presented using the SD-SDT model where the binding energy for Po^- was recalculated with SDT substitutions in the RCI calculation. The result from the single calculation made with core-valence correlation is given at the end.

5.1. The SD-SD model

New layers of correlation orbitals were added to the model until a satisfying degree of convergence for the EA was obtained. The orbitals which were optimized at each step are given in table 6. When the difference between the $\Delta x = 0$ case and the $\Delta x = 1$ case was less than 0.03 eV, the EA was considered to have converged. After expanding the AS to include the correlation orbitals up to and including $\{9s, 9p, 9d, 8f, 7g, 7h\}$, the difference between the $\Delta x = 0$ case and the $\Delta x = 1$ case was less than 0.03 eV. The convergence of the EA as more correlation orbitals were added is visualized in fig. 11. The binding energies and the corresponding EA for the different steps are displayed in table 7. The values presented in table 7 were obtained using MCDHF and RCI, meaning that the Breit interaction and additional QED effects were considered. By taking the average of the last value of the EA for the $\Delta x = 0$ case and $\Delta x = 1$ case, the EA was estimated to be 1.392 eV.

Table 6: The orbitals which were optimized at each step.

Step x	Optimized orbitals	Substitutions
1. MR	$1s, 2s, 2p, 3s, 3p, 3d, 4s, 4p, 4d,$ $5s, 5p, 4f, 5d, 6s, 6p\ 5f, 6d$	none
2. VV1	$7s, 7p, 7d, 6f, 5g$	SD
3. VV2	$8s, 8p, 8d, 7f, 6g, 6h$	SD
4. VV3	$9s, 9p, 9d, 8f, 7g, 7h$	SD

Table 7: The total binding energy E obtained at each step and the corresponding number of CSF's generated. The binding energies were obtained from calculations using MCDHF+RCI. The electron affinity is given both for the $\Delta x = 0$ cases and the $\Delta x = 1$ cases.

	Po		Po^-		EA [eV]	
Step x	NCSF	E [eV]	NCSF	E [eV]	$\Delta x = 0$	$\Delta x = 1$
1. MR	56	-603706.5587	45	-603707.1904	0.63172	
2. VV1	41 632	-603708.0207	55 628	-603709.2844	1.26369	2.72573
3. VV2	154 978	-603708.1831	205 638	-603709.5405	1.35735	1.51971
4. VV3	341 506	-603708.2118	451 914	-603709.5895	1.37768	1.40641

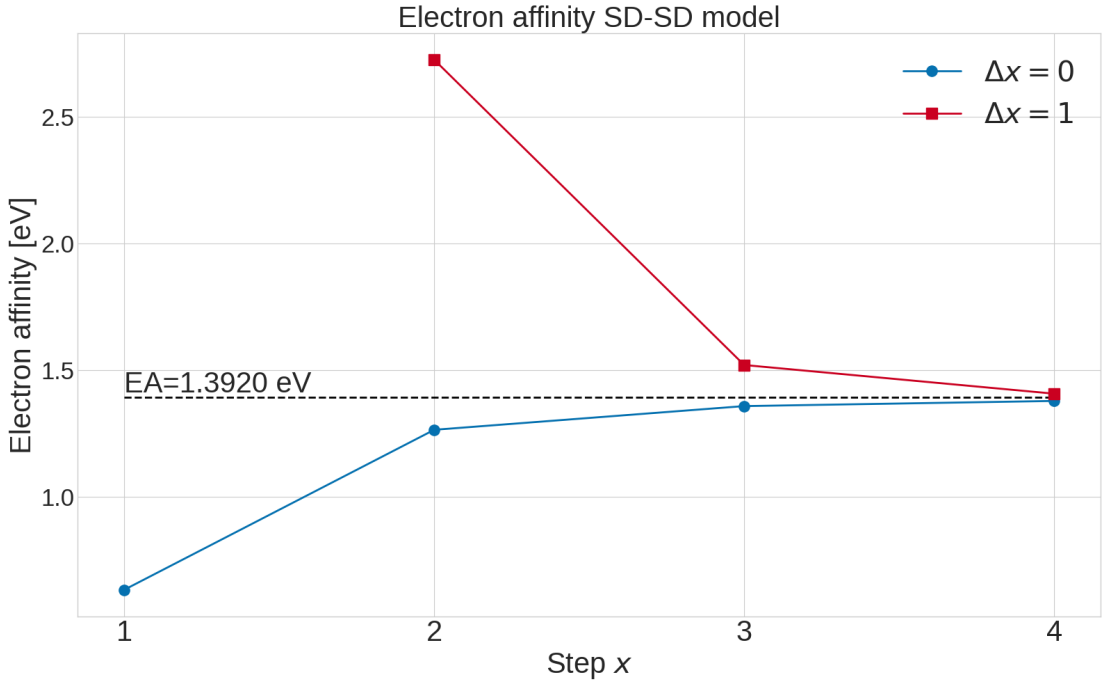

Figure 11: The electron affinity for the $\Delta x = 0$ case and the $\Delta x = 1$ case obtained at each step as given in table 7. At the last step, the $\Delta x = 0$ case and the $\Delta x = 1$ case are less than 0.03 eV apart with the average value of the EA being approximately 1.3920 eV.

5.2. The SD-SDT model

The attractive potential that keeps the electrons bound in the negative system is primarily a result from electron correlation. Therefore, it is theoretically predicted that the EA will be underestimated when using the same correlation models for Po and Po^-. To test this prediction, the convergence of the binding energy for the anion and the neutral atom were compared as more correlation orbitals were added. It is viewed in table 7 that

the difference between the first and last estimate of the binding energy is 1.6531 eV for Po and 2.3991 eV for Po^-. This indicated that more correlation needed to be included in the model for the anion compared to the neutral atom. Without having to reoptimize the radial orbitals, additional correlation effects were included in the model for Po^- by extending the list of CSF's used in the RCI calculation by allowing triple substitutions. With this new model for Po^-, the difference between the first and last estimate of the binding energy is 1.8436 eV. The difference in the binding energy between consecutive steps for Po and Po^- using the two different models is given in table 8. Between the two first steps, the binding energy of Po^- was lowered with 2.094 eV in the SD-SD model while in the SD-SDT model, the corresponding decrease was 1.5175 eV. For the next two steps, the difference in the binding energy was actually slightly larger for the SD-SDT model compared to the SD-SD model.

Table 8: The difference in the binding energy $\Delta E(x) = \big[E(x) - E(x-1)\big]$ between step x and step $(x-1)$.

Step x	Po SD $\Delta E(x)$ [eV]	Po^- SD $\Delta E(x)$ [eV]	Po^- SDT $\Delta E(x)$ [eV]
2	-1.462	-2.094	-1.5175
3	-0.1624	-0.2561	-0.2752
4	-0.0287	-0.0490	-0.0509

The EA was recalculated by taking the difference between the binding energies obtained for Po using the SD-SD model and the new values of the binding energy for Po^- using the SD-SDT model. The results are viewed in table 9. The number of CSF's was manageable with SDT substitutions up to and including the orbitals $\{8s, 8p, 8d, 7f, 6g, 6h\}$. When adding the next layer of correlation orbitals $\{9s, 9p, 9d, 8f, 7g, 7h\}$ the number of CSF's generated was 13 605 286 and the matrix elements could not be evaluated due to the size. Therefore, the last step in table 9 corresponds to SDT substitutions to the second layer of correlation and SD substitutions to the the third layer. The convergence of the EA in the SD-SDT model is visualized in fig. 12.

Table 9: The total binding energy E and number of CSF's obtained at each step for Po^- after recalculating the mixing coefficients with SDT substitutions in the additional RCI calculation. The electron affinities were calculated by using the binding energy for Po from the corresponding step in table 7.

	Po^-		EA [eV]	
Step x	NCSF	E [eV]	$\Delta x = 0$	$\Delta x = 1$
1.MR(SDT)	9 599	-603707.8025	1.24377	
2.VV1(SDT)	541 268	-603709.3200	1.29929	2.76133
3.VV2(SDT)	4 079 764	-603709.5952	1.41213	1.57450
4.VV2(SDT)+VV3(SD)	4 326 040	-603709.6461	1.43427	1.46299

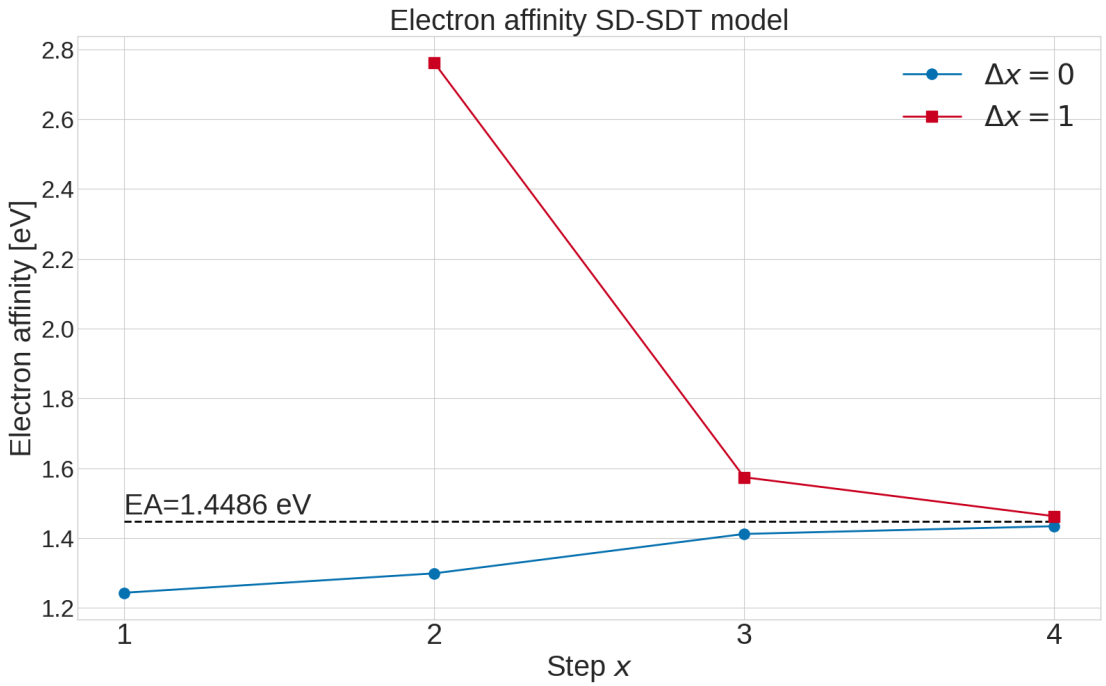

Figure 12: The electron affinity for the $\Delta x = 0$ case and the $\Delta x = 1$ case obtained at each step as given in table 9. At the last step, the $\Delta x = 0$ case and the $\Delta x = 1$ case are less than 0.03 eV apart with the average value of the EA being approximately 1.4486 eV.

A simple extrapolation was performed with an exponential fit on the form $f(x) = Ae^{-Bx} + C$ to the binding energies at each step in table 7 and table 9. The binding energies and the corresponding curves are plotted in fig. 13. The large difference in the first step between the two different models for Po^- is explained by the fact that no substitutions were allowed in the SD-SD model in the first step while SDT substitutions were included in the SD-SDT model. In the next three steps, SD substitutions were allowed in the SD-SD model. This large shift in the initial estimate of the binding energy will affect the general shape of the extrapolated curve for Po^- in fig. 13.

An extrapolated value of the EA for both the SD-SD model and the SD-SDT model were obtained by taking the difference between the exponential fit for Po(SD) and Po^-(SD) and the difference between Po(SD) and Po^-(SDT), respectively. The corresponding curves obtained from the SD-SD model and the SD-SDT model are viewed in fig. 14. With this extrapolation, the SD-SD model will estimate the EA to be 1.378 eV and the SD-SDT model will give an estimate of 1.446 eV.

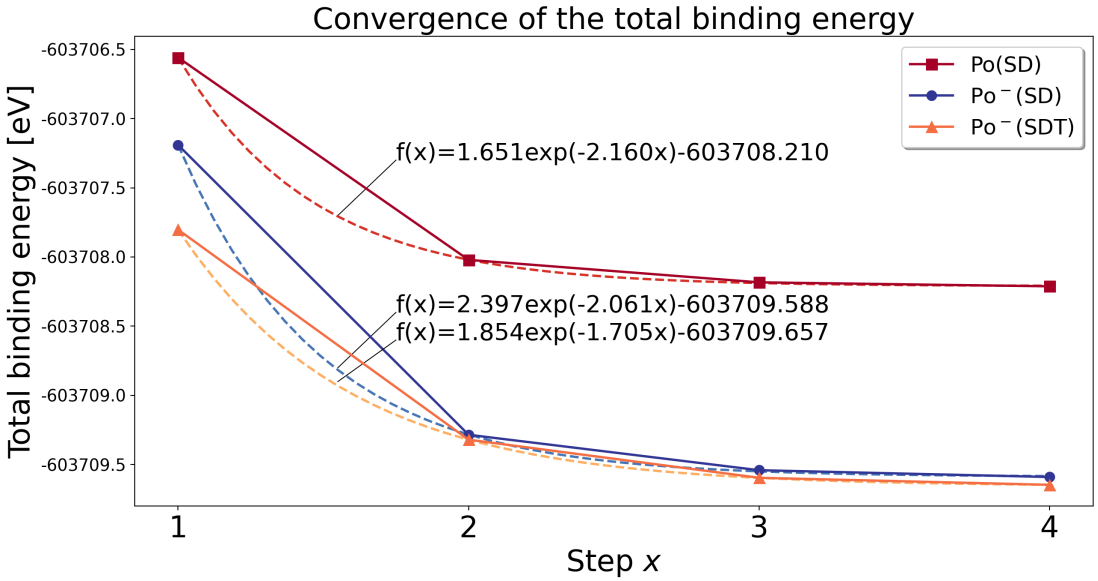

Figure 13: The solid curves correspond to the binding energies obtained at each step for Po and Po^- using the SD-SD model in table 7, as well as the binding energy for Po^- with the SD-SDT model in table 9. The dashed curves are exponential functions on the form $f(x) = Ae^{-Bx} + C$ fitted to the datapoints.

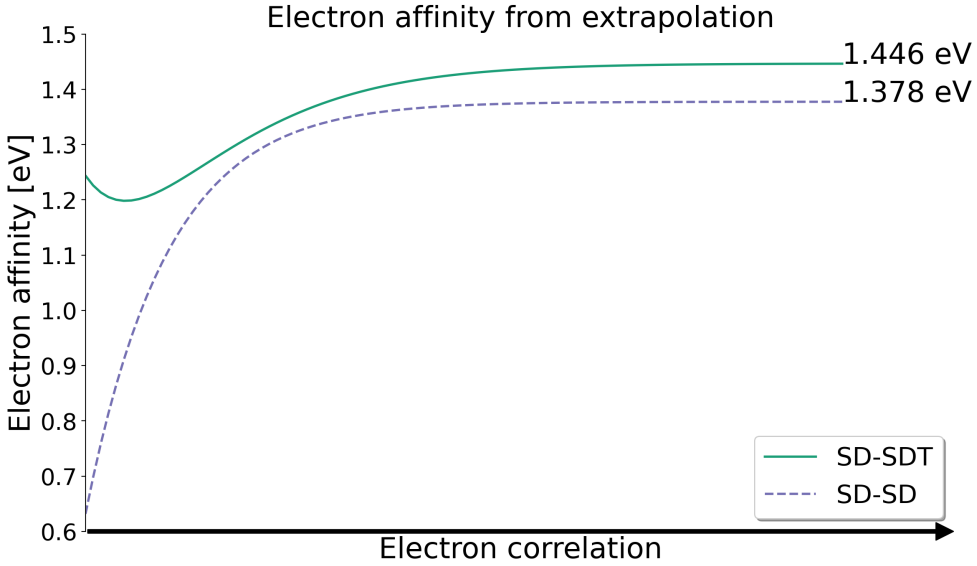

Figure 14: The two curves represent the EA which is obtained from taking the difference between exponential functions fitted to the binding energies (viewed in fig. 13). The SD-SD model approach a value of 1.378 eV for the EA while the SD-SDT model approach a value of 1.446 eV for the EA.

5.3. Including core-valence correlation

The estimate of the EA can be improved by including core-valence correlation. From the shape of the plotted orbitals in fig. 10 and the values found in table 3, it was decided to open up the orbitals $\{5s, 5p, 5d\}$. It was not possible to perform the calculations with substitutions to the third layer of correlation orbitals $\{9s, 9p, 9d, 8f, 7g, 7h\}$ since the number of CSF's grew to large. Therefore, it was decided to perform a calculation with VVC to the third layer of correlation and CVC to the second layer $\{8s, 8p, 8d, 7f, 6g, 6h\}$. The total binding energy for the ground state of Po was calculated to -603711.7217 eV and the corresponding energy for the negative ion Po^- was calculated to -603712.7951 eV. Given these two values, the electron affinity for the $\Delta x = 0$ case is 1.07345 eV which is almost 0.3 eV lower if compared to the estimate with only VVC. When adding a new correlation effect, it is important to make sure that the EA is converging. But with the current model, it was impossible to properly study the convergence due to the large number of CSF's. Likewise, it would not have been possible to study the effect of CVC while at the same time allowing triple substitutions in the model for Po^-. Therefore, this single value alone is unreliable but indicates that the electron affinity would be lowered if CVC was taken in to account. This is left for future studies.

6. Discussion

This section begins with a short discussion about the difficulties with balancing correlation between Po and its corresponding anion Po^-. This is followed by a comparison of the results presented in this report with earlier calculations of the EA of Po. A brief outlook on possible ways to extend and hopefully improve the model for future calculations is given at the end.

6.1. Balancing correlation

One of the main considerations when calculating the electron affinity is how to balance the correlation between the neutral atom and the anion, respectively. In the initial results from the calculations with only VVC and SD substitutions for both Po and Po^-, an EA of 1.392 eV was obtained. This value was found to be in the lower span when compared to prior calculations performed on Po. This observation led to further investigations of correlation effects. As more correlation orbitals were added to the models, it became apparent that the total binding energy for Po^- was more affected compared to Po, as shown in fig. 13. This indicated that more correlation had to be included in the model for Po^-. To achieve this without having to reoptimize the orbitals, the list of CSF's used in the RCI calculation was extended to include SDT substitutions.

As a result of the non-existent experimental value, it is difficult to determine whether the present calculated EA was improved when allowing SDT substitutions in the RCI calculation for the anion. Nevertheless, the fact that the binding energy of the neutral atom converged more quickly suggests that the system was unbalanced and without sufficient correlation treatment for the anion, the estimate of the EA would probably be too low. Having SDT substitutions in the additional RCI calculation produced a significant shift in the energy. However, if the shift in the energy leads to the EA being over- or undercompensated can not be determined at this stage. If SDT substitutions instead were used selectively in the SCF procedure, it is likely that a slightly different result on the binding energies would have been obtained.

6.2. Comparison to prior calculations

In table 10, values of the EA obtained from earlier studies are displayed. The study using MCDHF performed by Li *et al.* gave an estimate of 1.405 eV for the EA [7]. Even though the same method (MCDHF) was used, the systematic approach to add correlation was much different compared to the procedure employed in this report. In their model, only the $6p$-orbital was considered to be valence and the leading configuration was used as a single reference. The MCDHF procedure was not combined with additional RCI calculations, meaning that neither the Breit interaction nor leading QED effects were accounted for. The results presented in this report have improved the accuracy on all these parameters. Unlike the prior value where only the $6p$-orbital was considered to be valence, this model allowed substitutions both from the $6s$- and $6p$-orbitals by

which more correlation was included. Likewise, the MR was expanded to consist of four configurations for both Po and Po^-, respectively. Furthermore, the MCDHF procedure was combined with additional RCI calculations where both the Breit interaction and QED effects were included.

Table 10: Prior calculations of the electron affinity for Po.

EA [eV]	Method	Ref.
1.225	4c-MBPT	[8]
1.405	MCDHF	[7]
1.4696	CCSD(T)	[6]
1.9(3)	SE	[9]
1.446	MCDHF	This work

In the SD-SD model, the correlation was not differently balanced between Po and Po^-, and the EA was calculated to 1.392 eV. Using this model yielded an estimate of the EA 0.013 eV below the value obtained in the calculation with MCDHF performed by Li *et al.*. In their model, SDT substitutions to orbitals with $n = 6$ were included in the SCF procedure for Po^- and only SD substitutions for Po, unlike the model used in this project where only SD substitutions were allowed both for the anion and the neutral atom. By comparing the electron affinities, it is possible to conclude that the more extensive model used in this project yields a similar result for the EA compared to when the less extensive model was used with the correlation being unevenly balanced between Po and Po^-. In the SD-SDT model, the mixing coefficients were recalculated with SDT substitutions in the RCI calculation for Po^- and with an extrapolation of the binding energies, the EA was estimated to be 1.446 eV.

With the coupled-cluster method CCSD(T) combined with RCI, Borschevsky *et al.* have predicted the value 1.496 eV for the EA [6]. Prior calculations with CCSD(T) have for some systems proven good agreement with experimental results. For example with Bi using the same CCSD(T) method and procedure as with Po, the difference between the calculated value and the experimental result was only 0.05 eV [6]. This indicates that a similar agreement could be expected in the case of Po.

The CCSD(T) procedure used by Borschevsky *et al.* will typically underestimate the EA while the method employed by Li *et al.* will tend to overestimate the EA [28]. This is explained by Borschevsky *et al.* using the same correlation models for Po and Po^- while Li *et al.* include triple substitutions in the first steps for Po^- but not for Po. Applying this line of reasoning to this work, the value obtained from the SD-SDT model should overestimate the EA and the value computed from the SD-SD model should underestimate the EA. However, the expected relation between CCSD(T) and MCDHF is not observed for Po and instead, the CCSD(T) value is close to 0.07 eV above the value calculated by Li *et al.*. This may indicate that certain considerations should be taken

into account when performing atomic structure calculations on Po. It may be necessary to include more configurations in the MR and allow substitutions to higher order orbitals to achieve a representative value of the EA for Po.

The SD-SD model provides a lower baseline for the EA of 1.392 eV; it is however likely that this model underestimates the EA since the anion is more sensitive to electron correlation. Using the SD-SDT model with extrapolation gives a value of 1.446 eV. This shows that the additional RCI calculation have a significant effect on the EA when SDT substitutions are allowed in the model for Po^-. It would be interesting to study the effect on the EA with selective SDT substitutions in the SCF procedure for the anion but using an MR and with both the $6s$- and $6p$-orbitals as valence. With the MR selected in this project, it should also be considered whether the model would benefit from treating the $5f$- and $6d$-orbitals as valence. If such a calculation did yield a value of the EA above 1.40 eV, it would indicate that the model used by Li *et al.* was insufficiently small. However, such a study would be difficult to pursue due to the large sizes of the calculations. Even though more correlation effects are added in the model for the anion Po^-, the value calculated using the SD-SDT model is still 0.02 eV below the value obtained from CCSD(T). This result does not follow the expected behaviour and it would be interesting to understand this discrepancy.

6.3. Computational considerations

The main limitation of the project was the increasing sizes of the calculations as the configuration space was extended. Limited interactions were employed for the higher correlation layers in the SCF procedure through the use of Brillouin Wigner perturbation theory. For the additional RCI calculation, full interactions were considered and the expansion coefficients were successfully calculated when the number of CSF's was below 4.5 millions. With the computational resources available in this work, the `rci` program was unable to compute the integrals when the number of CSF's surpassed 6 millions. The best way of ensuring that the computations can be run is to limit the size of the configuration space. It is inevitable that the configuration space will grow as more correlation effects are included, but it is possible to reduce the number of CSF's by making wise choices in regards to which orbitals to optimize and at which step. This will require a more thorough analysis of which correlation orbitals are the most important to include for the neutral atom and the negative ion, respectively. To successfully account for CVC in the calculations, it will be necessary to use a model where fewer CSF's are generated at each step.

The later parts of the project was run on a HPC cluster. However, the performance was not as good as expected when running the codes. It proved to be difficult to fully utilize the CPU and RAM due to the internal structure of the `rci` program. Even though the memory was large enough to handle the calculations, the amount of disc space needed in order to run the calculations became an issue. The `rci` program uses files written to the disc for internal communication and for large scale calculations will

require many hundreds of GB. It is possible that the performance could be slightly improved by optimizing the compilation of the codes to the particular nodes used at Vera.

7. Conclusions and outlook

The aim of the project was to calculate a new estimate of the electron affinity (EA) of Po. The computations were performed using the MCDHF method combined with complementary RCI calculations. A model was constructed by performing initial calculations with the intention to define a suitable multi-reference and identify which orbitals should be considered valence. Electron correlation was included in the model by allowing SD substitutions to a set of correlation orbitals. The set of orbitals was expanded until the value of the EA had converged. Using this model, the EA was estimated to be 1.392 eV. Both from theoretical considerations and calculations performed in this project, it was hypothesized that additional correlation effects needed to be included in the model for the anion Po^-. This was achieved by allowing SDT substitutions in the additional RCI calculation for the anion Po^-. In this new model with SDT substitutions for Po^-, the EA was estimated to 1.446 eV, which is our final value for the Po electron affinity for this study.

In hindsight, we can motivate the SDT treatment of the Po^- system by comparing the impact of correlation in the SD-SD model. Judging from the values in table 7 and table 9 and as visualized in fig. 13, it is clear that the anion is more affected by an increased correlation space. However, when comparing the final total binding energies with those from the DHF calculations in table 1, the atom somewhat unexpectedly has a larger correlation contribution by ca 1 eV. This is not the expected result since anions are known to be more sensitive to electron correlation effects. This can be explained by the more open $6p^4$ valence shell as compared to the $6p^5$ of the anion, which can be seen as a single electron hole. In other words, the atom has a larger valence shell, in general leading to more interactions within the same shell (in our case $n = 6$). Nevertheless, this indicates that further tests of the correlation models might be desirable.

Looking ahead, it would be interesting to do some modifications to the model and study how the EA would be affected. However, before any experimental value of the EA is available, it is impossible to determine how well certain models or methods can predict the EA. Under the assumption that the upcoming experiment succeeds in measuring the EA of Po, a natural next step would be to measure the isotope shift on the EA. But any such experiments would be preceded with theoretical calculations estimating the isotope shift. Therefore, another possible extension of this project would be to perform additional isotope shift calculations on the Po and Po^- ground terms.

References

[1] J. J. Thomson, "Bakerian lecture: rays of positive electricity", Proceedings of the Royal Society of London. Series A, Containing Papers of a Mathematical and Physical Character **89**, 1–20 (1913).

[2] D. J. Pegg, "Structure and dynamics of negative ions", **67**, 857–905 (2004).

[3] T. J. Millar, C. Walsh, and T. A. Field, "Negative ions in space", Chemical Reviews **117**, PMID: 28112897, 1765–1795 (2017).

[4] M. Kristiansson, K. Chartkunchand, G. Eklund, O. Hole, E. Anderson, N. de Ruette, M. Kaminska, N. Punnakayathil, J. Navarro-Navarrete, S. Sigurdsson, J. Grumer, A. Simonsson, M. Björkhage, S. Rosén, P. Reinhed, M. Blom, A. Källberg, J. Alexander, H. Cederquist, and D. Hanstorp, "High-precision electron affinity of oxygen", Nature Communications **13**, 5906 (2022).

[5] M. Nichols, M. Athanasakis-Kaklamanakis, Y. Balasmeh, A. Borschevsky, T. E. Cocolios, R. Crosa-Rossa, R. P. de Groote, C. Fajordo-Zambrano, K. T. Flanagan, R. F. Garcia Ruiz, D. Hanstorp, Á. Koszorús, l. Lalanne, D. Leimbach, Y. C. Liu, Y. S. Liu, K. M. Lynch, A. McGlone, G. Neyens, F. Pastrana, J. Reilly, S. Rothe, J. Trujillo, B. van den Borne, S. G. Wilkins, and X. F. Yang, *Measuring the electron affinity of polonium*, tech. rep. (CERN, Geneva, 2023).

[6] A. Borschevsky, L. F. Pašteka, V. Pershina, E. Eliav, and U. Kaldor, "Ionization potentials and electron affinities of the superheavy elements 115–117 and their sixth-row homologues bi, po, and at", Phys. Rev. A **91**, 020501 (2015).

[7] J. Li, Z. Zhao, M. Andersson, X. Zhang, and C. Chen, "Theoretical study for the electron affinities of negative ions with the mcdhf method", Journal of Physics B: Atomic, Molecular and Optical Physics **45**, 165004 (2012).

[8] T. Zeng, D. G. Fedorov, and M. Klobukowski, "Multireference study of spin-orbit coupling in the hydrides of the 6p-block elements using the model core potential method", The Journal of Chemical Physics **132**, 074102 (2010).

[9] R. J. Zollweg, "Electron affinities of the heavy elements", The Journal of Chemical Physics **50**, 4251–4261 (1969).

[10] D. Griffiths, *Introduction to electrodynamics* (Pearson Education, 2014).

[11] M. Kristiansson, *Precision measurements on negative ions* (Department of Physics, Stockholm University, 2022).

[12] P. Andersson, A. O. Lindahl, C. Alfredsson, L. Rogström, C. Diehl, D. J. Pegg, and D. Hanstorp, "The electron affinity of phosphorus", Journal of Physics B: Atomic, Molecular and Optical Physics **40**, 4097–4107 (2007).

[13] *Wikipedia: electron affinity (data page)*, [Online; accessed Oct 2022], `https://en.wikipedia.org/wiki/Electron_affinity_%28data_page%29`.

[14] S. Andersson, F. Bruhn, J. Hedman, L. Karlsson, S. Lunell, K. Nilson, and J. Wall, *Atom- och molekylfysik* (Fysiska institutionen Uppsala universitet, 2005).

[15]T. Brage, C. Froese-Fischer, and P. Jonsson, *Computational atomic structure: an mchf approach*, English (Routledge, 2022;2019;).

[16]R. D. Cowan, *The theory of atomic structure and spectra*, en, Los Alamos series in basic and applied sciences 3 (University of California Press, Berkeley, 1981).

[17]A. Hibbert, *Lecture notes in computational atomic physics* (School of Mathematics and Physics Queen's University Belfast, 2022).

[18]A. Rauk, *Orbital interaction theory of organic chemistry* (Wiley, 2004).

[19]J. Grumer, *Theoretical atomic spectroscopy of eartbound and stellar plasma* (Lund University, 2016).

[20]H. Haken, W. Brewer, and H. Wolf, *The physics of atoms and quanta: introduction to experiments and theory*, Advanced Texts in Physics (Springer Berlin Heidelberg, 2006).

[21]A. Kramida, Y. Ralchenko, and J. Reader, *Nist atomic spectra database*, [Online; accessed Oct 2022], https://www.nist.gov/pml/atomic-spectra-database.

[22]C. Froese Fischer, G. Gaigalas, P. Jönsson, and J. Bieroń, "Grasp2018—a fortran 95 version of the general relativistic atomic structure package", Computer Physics Communications **237**, 184–187 (2019).

[23]A. Papoulia, *Computational atomic structure: applications to astrophysics and nuclear structure* (Mathematical Physics, Lund University, Feb. 2020).

[24]R. Si, S. Schiffmann, K. Wang, C. Y. Chen, and M. Godefroid, "Ab initio multiconfiguration dirac-hartree-fock calculations of the in and tl electron affinities and their isotope shifts", Phys. Rev. A **104**, 012802 (2021).

[25]*Chalmers centre for computational science engineering*, [Online; accessed Jan 2023], https://www.c3se.chalmers.se/.

[26]J. J. Sakurai and J. Napolitano, *Modern quantum mechanics*, 3rd ed. (Cambridge University Press, 2020).

[27]A. Kramida, Y. Ralchenko, and J. Reader, *Nist atomic spectra database*, [Online; accessed Feb 2023], https://physics.nist.gov/cgi-bin/cuu/Value?hrev.

[28]R. Si and C. F. Fischer, "Electron affinities of at and its homologous elements cl, br, and i", Physical Review A **98**, 10.1103/physreva.98.052504 (2018).

Appendices

A. Evaluation of $\langle r^s \rangle$

We wish to explicitly calculate expectation values $\langle r^s \rangle$ for integer values of s for hydrogen-like ions. Since the electron is moving in a spherical Coulomb potential, the second derivative $P''_{nl}(r)$ w.r.t. r will relate to $P_{nl}(r)$ according to [14, pp. 64−70]

$$P''_{nl} = \left[\frac{l(l+1)}{r^2} - \frac{2Z}{a_0 r} + \frac{Z^2}{n^2 a_0^2} \right] P_{nl}. \tag{40}$$

Since P_{nl} is real-valued, eq. (40) can be multiplied with $P_{nl} r^s$ to obtain

$$\int_0^\infty P_{nl} r^s P''_{nl}\, dr = l(l+1)\langle r^{s-2} \rangle - \frac{2Z}{a_0} \langle r^{s-1} \rangle + \frac{Z^2}{n^2 a_0^2} \langle r \rangle. \tag{41}$$

The integral containing P_{nl} and it's second derivative P''_{nl} can be evaluated through integration by parts and with the requirement that P_{nl} goes to zero for $r \to 0$ and $r \to \infty$. An explicit calculation of the integral will give

$$\int_0^\infty P_{nl} r^s P''_{nl}\, dr = -\frac{l(l+1)(s-1)}{(s+1)} \langle r^{s-2} \rangle + \frac{2sZ}{a_0(s+1)} \langle r^{s-1} \rangle - \frac{Z^2}{n^2 a_0^2} \langle r \rangle + \frac{s(s-1)}{2} \langle r^{s-2} \rangle. \tag{42}$$

Setting the LHS equal to the RHS in eq. (40) and rearranging the terms will yield the Kramer's relation

$$\frac{s+1}{n^2} \langle r^s \rangle - (2s+1) \frac{a_0}{Z} \langle r^{s-1} \rangle + s \left[l(l+1) + \frac{1-s^2}{4} \right] \frac{a_0^2}{Z^2} \langle r^{s-2} \rangle = 0. \tag{43}$$

Since the wave function is normalized $\langle r^0 \rangle = 1$ and setting $s = 0$ gives

$$\left\langle \frac{1}{r} \right\rangle = \frac{Z}{n^2 a_0}. \tag{44}$$

The Hellman-Feynman theorem gives the expectation value of $\langle r^{-2} \rangle$ [26]

$$\left\langle \frac{1}{r^2} \right\rangle = \frac{Z^2}{(l+\frac{1}{2}) n^3 a_0^2}. \tag{45}$$

Finally, setting $s = -1$ and using the results from eq. (44) and eq. (45) yields the expectation value

$$\left\langle \frac{1}{r^3} \right\rangle = \frac{Z^3}{l(l+\frac{1}{2})(l+1) n^3 a_0^3}. \tag{46}$$

B. Example of batch script

```
#!/usr/bin/env bash
#SBATCH -A C3SE2023-1-7 -p vera
#SBATCH -C ICELAKE
#SBATCH -n 64
#SBATCH -t 2-00:00:00
#SBATCH --mail-user=gusarmly@student.gu.se
#SBATCH --mail-type=end

module load foss

cp $HOME/calcs/bachelor/Po_6p5/CV2/run_rci_6p5_CV2.sh $TMPDIR
cp $HOME/calcs/bachelor/Po_6p5/CV2/run_create_disks.sh $TMPDIR
cp $HOME/calcs/bachelor/Po_6p5/VV3/isodata $TMPDIR
cp $HOME/calcs/bachelor/Po_6p5/VV3/Po_6p5_AS3.w $TMPDIR

cd $TMPDIR
mkdir grasp_tmp_mpi

./run_create_disks.sh
cp disks $SLURM_SUBMIT_DIR
./run_rci_6p5_CV2.sh

cp Po_6p5_CV2.csum $SLURM_SUBMIT_DIR
cp Po_6p5_CV2.cm $SLURM_SUBMIT_DIR
```